LA-UR-80-1459
79p

TITLE: Computational Methods for LMFBR Whole-Core Accident Analysis

AUTHOR(S): M. G. Stevenson, Q-DO and J. F. Jackson, DAD/NRC

SUBMITTED TO: Chapter 16 in Proceedings of the International Centre for Heat and Mass Transfer 1980 Summer School and International Seminar

Dubrovnik, Yugoslavia

MASTER

University of California

LOS ALAMOS SCIENTIFIC LABORATORY
Post Office Box 1663 Los Alamos, New Mexico 87545
An Affirmative Action/Equal Opportunity Employer

Form No. 836 R3
St. No. 2629
12/78

UNITED STATES
DEPARTMENT OF ENERGY
CONTRACT W-7405-ENG 36

COMPUTATIONAL METHODS FOR LMFBR WHOLE-CORE ACCIDENT ANALYSIS*

M. G. Stevenson and J. F. Jackson
Los Alamos Scientific Laboratory
University of California
Los Alamos, New Mexico USA

ABSTRACT

This chapter discusses the development of current state-of-the-art computational methods used in the United States for analysis of core meltdown accidents (Hypothetical Core Disruptive Accidents) in LMFBRs. The emphasis is on the phenomenological basis and numerical methods of the codes SAS, VENUS-II, SIMMER and REMCO.

1. INTRODUCTION

The development of computational methods for Liquid-Metal Cooled Fast-Breeder Reactor (LMFBR) accident analysis has long been dominated by the difficult problem of core melt, disassembly, and possible primary system damage. Although other LMFBR analysis methods also are important in assuring public safety, this chapter will discuss only the computer methods used in the mechanistic analysis of LMFBR core meltdown, i.e., the Hypothetical Core Disruptive Accident (HCDA).

Over 20 years of development from the initial Bethe-Tait method[1] have provided increasingly complex computer codes that tax the fastest computers available. These codes synthesize the ever improving understanding of basic accident phenomena into a consistent analytical framework based on fundamental conservation laws. Experience has shown that many of these phenomena are complex and highly interactive (see Chapters 14-16). Furthermore, our understanding of them rests largely on small-scale experiments that often are performed with simulant materials. In many cases, direct experimental data are unobtainable. Thus, large mechanistic codes must be able to provide reliable and comprehensive predictions of full-scale accident behavior.

Because the primary sodium in an LMFBR operates at low (nearly atmospheric) pressure, system design can preclude a complete loss of coolant and core uncovering as the initiator of a whole-core melt. The only accident initiators that can lead to whole-core melt are (1) transients combined with failure to shut down (scram), (2) shutdown loss of decay heat removal, (3) core-wide failure propagation (such as initiated by local flow blockages), and (4) rapid and large reactivity insertions exceeding protective system response. Proper design can

*Work performed under the auspices of the US Nuclear Regulatory Commission and the US Department of Energy.

virtually eliminate all of these; but meltdowns initiated by at least one of these mechanisms are usually considered in licensing evaluations. In the US, the two transients that have received the most attention are the loss-of-flow and the transient overpower accidents.

Although many codes have been developed for HCDA analysis, we will concentrate on the phenomenological basis, numerical methods, and experimental verification of the major whole-core accident analysis codes or code series used in the US, i.e., SAS,[2-5] VENUS,[6,7] SIMMER,[8,9] and REXCO.[10] These or similar codes are being used in several countries for LMFBR HCDA analysis. Other US codes, such as MELT-III,[11] TWOPOOL,[12] and VENUS-III[13] provide important supplementary analysis capabilities, but will not be discussed in detail here.

It is extremely difficult to calculate in detail meltdown sequences from initiation through complete cessation of significant material motion in the primary system. Indeed, this goal has not yet been accomplished. However, the mechanistic methods noted above can now track sequences until neutronic events and the resulting energetics are largely over. For most cases, the primary remaining analysis problem is to assess the potential for melt-through of the vessel. Although the available methods provide a mechanistic framework for analyzing the energetics of accident sequences, there remain modeling limitations and uncertainties. There is a strong need for experimental verification, particularly of the modeling of the complex process of gradual core disruption. In addition, SAS and SIMMER are very long running. Their use in a production mode for many calculations is practical only on the largest computers.

2. CORE DISRUPTION ACCIDENT SEQUENCES

Before discussing the details of the codes noted above, it is useful to discuss their historical development as related to the phenomenology involved in whole-core-disruptive accident sequences. The details of core disruptive accident phenomenology are presented in Chapters 14-16. The purpose of this section is to review HCDAs from the viewpoint of mechanistic computer code development. In addition to the two-phase-flow phenomenology typical of Light-Water Reactor (LWR) accident analysis, LMFBR meltdown accident calculations must focus on reactivity events. Motion of any of the core materials (sodium, steel, fuel, and control) can have a significant reactivity effect. Fuel compaction, the concern of the original Bethe-Tait analysis,[1] has a potential for leading to severe excursions. Conversely, outward redistribution of fuel is the only way to achieve a permanently shutdown neutronic state unless control rods are inserted into the core during the accident sequence. The tight coupling of the complex material motions with reactivity effects demands considerable care in the modeling.

Until about 1973, HCDA sequences usually were analyzed in the four relatively unique phases, shown in Fig. 1 and discussed below.

2.1 Accident Initiation

This phase of a mechanistic accident analysis involves a calculation of the core neutronics and thermal behavior to the point of loss-of-subassembly geometry. Because most LMFBR designs use rigid subassembly ducts, intact subassemblies are coupled only through inlet and outlet thermal-hydraulic conditions and through reactor power. Subassemblies with similar power, flow, and irradiation conditions are generally, although not necessarily, lumped together in groups. All the subassemblies within a given group, or "channel," are

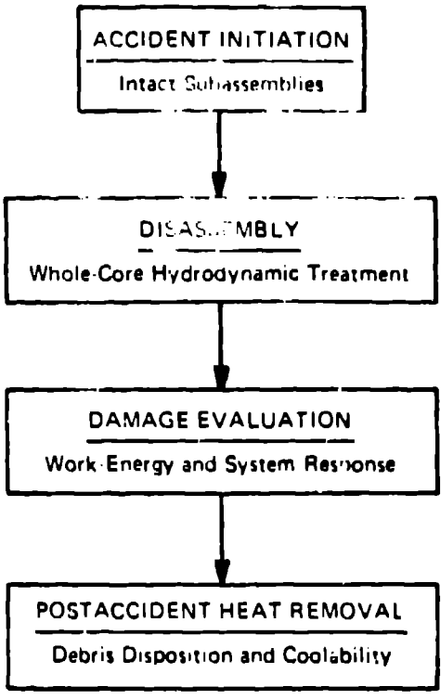

Fig. 1. Traditional approach to mechanistic accident analysis.

assumed to behave identically. Phenomena such as transient thermal-hydraulics, sodium boiling, fuel-pin mechanics and failure, cladding and fuel motion, and fuel-coolant interactions are treated with one-dimensional models Figure 2 depicts this kind of multichannel core representation.[14] The multichannel SAS codes (SAS2A and its successors) were preceded in the US by multichannel codes such as FREADM[15] and TART.[16] These earlier codes included simple parametric models, particularly of sodium voiding, and were designed to allow a reasonably

Fig. 2. Multichannel core representation in a one-dimensional model.

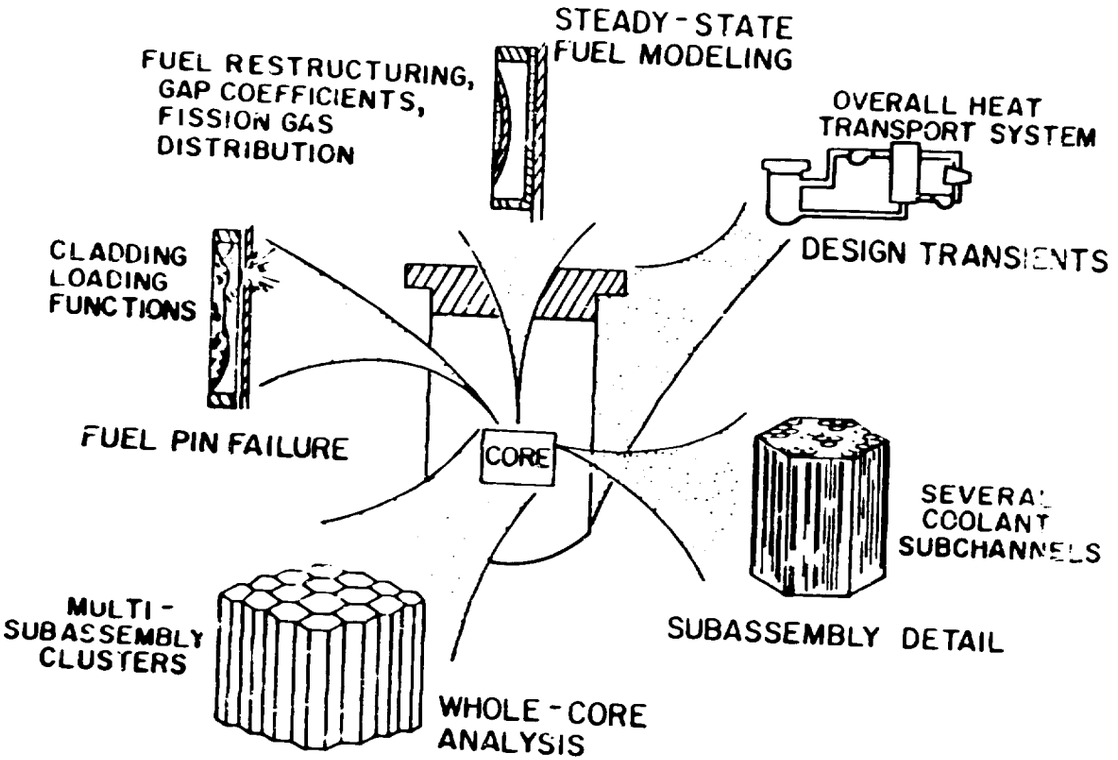
STEADY-STATE
FUEL MODELING
FUEL RESTRUCTURING,
GAP COEFFICIENTS,
FISSION GAS
DISTRIBUTION
OVERALL HEAT
TRANSPORT SYSTEM
DESIGN TRANSIENTS
CLADDING
LOADING
FUNCTIONS
FUEL PIN FAILURE
CORE
SEVERAL
COOLANT
SUBCHANNELS
SUBASSEMBLY DETAIL
MULTI-
SUBASSEMBLY
CLUSTERS
WHOLE-CORE
ANALYSIS

realistic but conservative accounting of reactivity effects for input to the core disassembly codes available in the late 60s, such as MARS.[17] At that time in the US, HCDA analysis was focused on 1000 MWe-sized reactors, and accident sequences were dominated by high reactivity insertion rates due to large, positive, sodium void worths. These early multichannel codes led to the recognition that a mechanistic treatment of noncoherence of sodium voiding among subassemblies of varying initial power and sodium flow was important.[18]

2.2 Disassembly Analysis

A "classical" disassembly typically begins when a prompt-critical neutronics excursion is induced. The resulting rapid heating and vaporization of the fuel produce relatively high pressures that disassemble the core, i.e., move the fuel outward rapidly, and thereby end the power burst. This disassembly process was first described by the Bethe-Tait model. In this approach, the core was treated as a homogeneous fluid so that the material motion during disassembly could be calculated using a hydrodynamic approach. The original Bethe-Tait calculations were done in spherical geometry. The reactor power was calculated using point kinetics with first-order perturbation theory to estimate the reactivity feedback associated with the material motion. Analytic approximations simplified the equations so that hand calculations could be made. The method was later codified in the Weak Explosion code.[19] At about the same time, methods using numerical solutions of one-dimensional hydrodynamics and neutron transport equations were developed, such as the AX-1 code.[20]

Variations and improvements[21] subsequently were made to the basic Bethe-Tait approach. Doppler feedback was included, improvements were made to the equation of state used to estimate the pressures, more accurate neutronics was implemented in some cases, and the capability for doing hydrodynamics calculations in two-dimensional (r,z) geometry was added. A number of disassembly computer codes were developed in the US as successive improvements were made, with VENUS-II[7] now being the most used of these classical disassembly codes.

2.3 Damage Evaluation

During or following reactor disassembly, the rate at which the thermal energy released in the transient can be converted to kinetic energy (work) must be established. This is needed to evaluate the damage that the excursion might cause to the system. Work can either come from the expansion of the core materials themselves or from the interaction of these materials with the sodium coolant causing its consequent vaporization and expansion. Early studies of the damage potential of core-disruptive accidents assumed that the work on the surrounding reactor structures would be done by the expanding fuel materials only. The maximum work potential was evaluated by isentropic expansion calculations.[22]

As larger oxide-fueled reactors were considered, it was recognized that the transfer of heat from the high-temperature fuel to the sodium could considerably increase the potential work available to do damage. Hicks and Menzies[23] calculated the maximum work potential that could result if heat transfer to the sodium were extremely rapid. Because very high heat-transfer rates had been observed in reactor accidents and experiments (SL-1, SPERT) attention turned to predicting these rates by assuming fragmentation of the fuel into sodium. Initially, this was done parametrically by varying the fuel particle size and mixing time and calculating the resulting heat-transfer rates as a basis for assessing damage potential. Early results of this type of calculation were

reported by Cho, et al.[24] and Padilla.[25] A review of the historical development of work-energy conversion is available in Ref. 26.

Once the pressure source term is established, the response of the system can be analyzed. This usually is done with a hydrodynamic calculation of the pressure propagation coupled with an analysis of the structural response of the important system components. The REXCO series[16] of codes is widely used in the US for this purpose. The initial versions of REXCO used hydrodynamics methods similar to those already in use[27] at the Los Alamos Scientific Laboratory (LASL) and Lawrence Livermore Laboratory (LLL).

2.4 Postaccident Heat Removal

The final phase in HCDA analysis (excluding containment and consequence analysis) is an evaluation of postaccident heat removal (PAHR). The objective is to analyze the long-term decay heat removal from the fuel following a disruptive accident. This has mainly taken the form of defining possible post-disruptive fuel dispositions and of analyzing the subsequent coolability. The disposition of core materials and the required measures to assure cooling of the core debris are, of course, dependent on the reactor design under consideration.

Detailed mechanistic analysis methods are not yet in common use for this problem and we will not discuss this area further. Reviews of the phenomenology are available in Ref. 28.

2.5 Gradual Core Disruption and the Transition Phase

The relatively clear-cut separation into the phases discussed above has disappeared with more detailed analyses. As initiating-phase models improved, the resulting initial nuclear excursions became progressively milder, largely due to the more accurate representation of intersubassembly noncoherence. This noncoherence arises mainly from carefully accounting for the differences in power level and coolant flow rates among the subassemblies. The net result of this is that calculated accident sequences tend to proceed into a gradual melt-down of the core, instead of ending in a vigorous disassembly excursion. This does not mean that a disassembly excursion cannot be induced at some point in the accident, but merely that it is unlikely in the early stages of core melt-down. Another important reason for considering milder accident progressions was the concentration in the US on the Fast Flux Test Facility (FFTF) and the Clinch River Breeder Reactor (CRBR) reactors with positive sodium void worths much smaller than the 1000-MWe reactors emphasized in the middle-to-late 1960s.

As an example, a characterization of the CRBR unprotected loss-of-flow (ULOF) accident (assuming a preirradiated core) consists of (1) undercooling of the core; (2) sodium boiling and mild power increase leading both to cladding melting and relocation and to cladding failures in partially voided and non-voided subassemblies; (3) fuel swelling, slumping, and/or dispersal driven by fission gas and sodium vapor; and (4) melting of subassembly cans initiating a "transition phase" of gradual disruption. This latter phase is characterized by steel relocation and vaporization and fuel melting and motion until no core fuel subassembly structures remain intact. In this kind of accident sequence, reactivity insertion rates from sodium boiling are only a few \$/s at the highest.[29] Similarly, cladding and fuel motion in intact subassemblies typically leads to at most a few \$/s. Even in larger reactors with large positive sodium

void reactivities, maximum positive voiding reactivity rates from normal boiling are given as only a few tens of \$/s[30] by SAS3A calculations.

The definition of the transition phase led to the more generic accident progression diagram shown in Fig. 3. The progression from initiating phase to a classical disassembly is included as is the gradual core disruption of the transition phase.

In the transition phase, a subassembly successively progresses through coolant voiding and melting, generating pressures generally too low to cause a massive dispersal of molten fuel from the core region. The subassembly can walls melt quickly, and growing regions of molten fuel and steel begin to form in the hottest portions of the core. This stage of the accident is likely to be accompanied by a number of mild excursions induced by continued slumping in successively lagging subassemblies and by the re-entry of fuel that was temporarily dispersed by mild pressurizations. Recent SIMMER-II calculations[31] indicate that excursions occur with only a few tens of \$/s for maximum reactivity insertion rates in the CRBR ULOF transition phase, but these increase as more subassemblies become involved.

The neutronic events in this sequence can be terminated by three mechanisms. First, the transition phase can end relatively benignly with gradual fuel removal

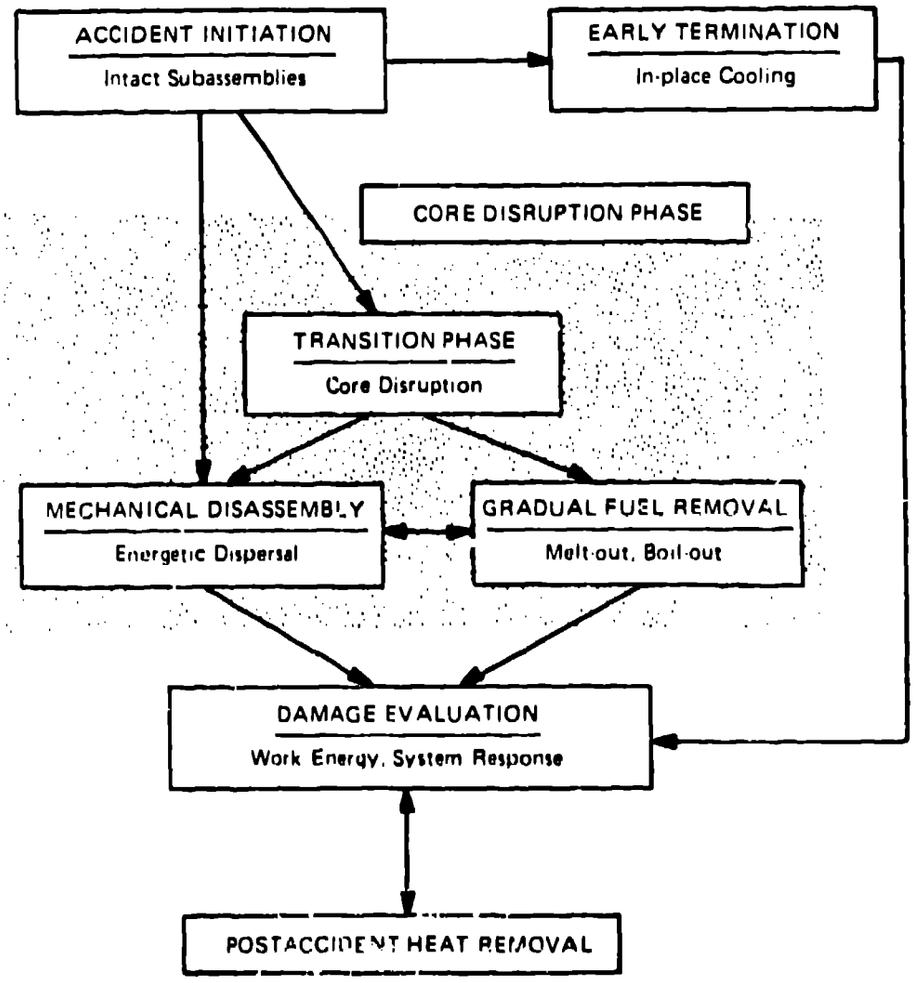

Fig. 3. Comprehensive accident progression diagram.

by mild expulsions, meltout processes, or both. Second, a bottled core blowdown can occur, in which a molten core completely contained by the surrounding structure gradually heats and pressurizes due to decay heat generation and/or mild neutronic bursts, then blows down (expands) following sudden opening (due to melt-through or mechanical failure) of the surrounding structure. Third, the rapid expansion following sufficiently energetic neutronic excursions can remove sufficient fuel from the core to leave the reactor permanently shut down.

A developing area of analysis has been the calculation of the extended motion or core expansion following either a disassembly-type excursion or a bottled-core blowdown. SIMMER-II calculations[32] of postdisassembly expansions have indicated considerably reduced thermal to-kinetic-energy (work) conversion efficiencies compared to the more conventional isentropic expansion calculations. SIMMER-II can bridge the analysis areas between SAS and REXCO because of its ability to (1) follow directly from SAS initiating-phase calculations into a transition phase (possibly including several neutronic excursions and progressing to a completely disrupted core,[31] (2) follow the extended material motion after these excursions, and (3) determine pressure loadings on the system.

A different path to terminating a disruptive accident sequence before either a disassembly or a transition phase was first noted during the analysis[33] of unprotected transient overpower accidents (UTOP) in the FFTF and is indicated by the "early termination" path in Fig. 3.

A UTOP accident can be characterized by (1) pins failing before any sodium boiling, (2) the ejection of molten fuel and fission gas into flowing liquid sodium, (3) localized voiding by expanding fission gas and sodium vaporization, (4) dispersal out of the active core of some of the ejected fuel, and (5) some freezing of molten fuel but incomplete plugging of coolant subchannels. If the reactivity insertion driving the overpower ceases, then the fuel sweepout can lead to a neutronically stable condition with in-place cooling of the remaining fuel debris and unfailed pins. Conversely, continuation of the driving reactivity or a lack of adequate in-place cooling could lead to whole-core involvement. If a transition phase developed, it would involve considerably different conditions than a ULOF because full coolant flow would continue, at least in unmelted channels, and all channels would experience the full-core pressure drop. Generally, transition phase behavior for a UTOP initiator has not been examined in any detail.

With the above as background, we now examine some of the specific codes. The following code descriptions include brief discussions of the numerical methods used to solve the equations. Some introductory information on numerical methods is presented in Appendix A. This includes defining some of the key terms used in the various code descriptions.

3. THE SAS ACCIDENT INITIATION CODES

The SAS codes represent a long development from the single-channel SAS1A version through SAS2A, SAS3A, SAS3D, and SAS4A (soon to be completed). This development, as for other LMFBR accident analysis methods, proceeded without the benefit of an adequate phenomenological data base. As might be expected, this resulted in some significant modeling deficiencies when compared to experimental data, although the successes[34,35] with some of the early models were gratifying given their ad hoc nature. The early models also have tended to lose credibility because of numerical deficiencies, particularly as their scope was extended into analyzing more slowly developing accident sequences. In the

initial developments, to quote Waltar and Padilla,[14] "attention to mathematical solutions was normally only given to the degree necessary for obtaining a stable and accurate, but not necessarily efficient, numerical solution."

SAS1A[2] was a single-channel code that included point reactor kinetics; a combination of annular slip two-phase flow and single-bubble slug-boiling models;[36] an elastic-plastic cladding and elastic-fuel deformation model, DEFORM-I;[37] a transient fuel-pin heat-transfer model; and an internal switch to the MARS[17] disassembly module.

The sodium-boiling model was later completely rewritten as a multibubble slug-boiling model for the multichannel SAS2A version.[3] A new fuel-pin deformation module, DEFORM-II,[38] also was included in a version of SAS2A. SAS2A did not include the MARS disassembly module but provided punched output that could be used as input for initial conditions in the VENUS-II disassembly code.

The phenomenological structure of SAS3A is shown in Fig. 4. SAS3A[4] contained the first models, such as CLAZAS,[39] SAS/FCI,[40] and SLUMPY,[41] to allow complete calculations of cladding and fuel motions into the transition phase. SAS3D used the same models but restructured the code for more numerical efficiency and to allow up to 35 channels instead of the 10 allowed in SAS3A. SAS4A[5] is a new code with a new sodium-boiling module and with CLAP,[42] PLUTO2,[43] and LEVITATE[44] replacing the equivalent models of SAS3A and SAS3D. Here we will concentrate on the developments through SAS3A but will relate the newer models of the not yet released SAS4A to the earlier ones as appropriate.

Fig. 4. SAS3A module relationships.

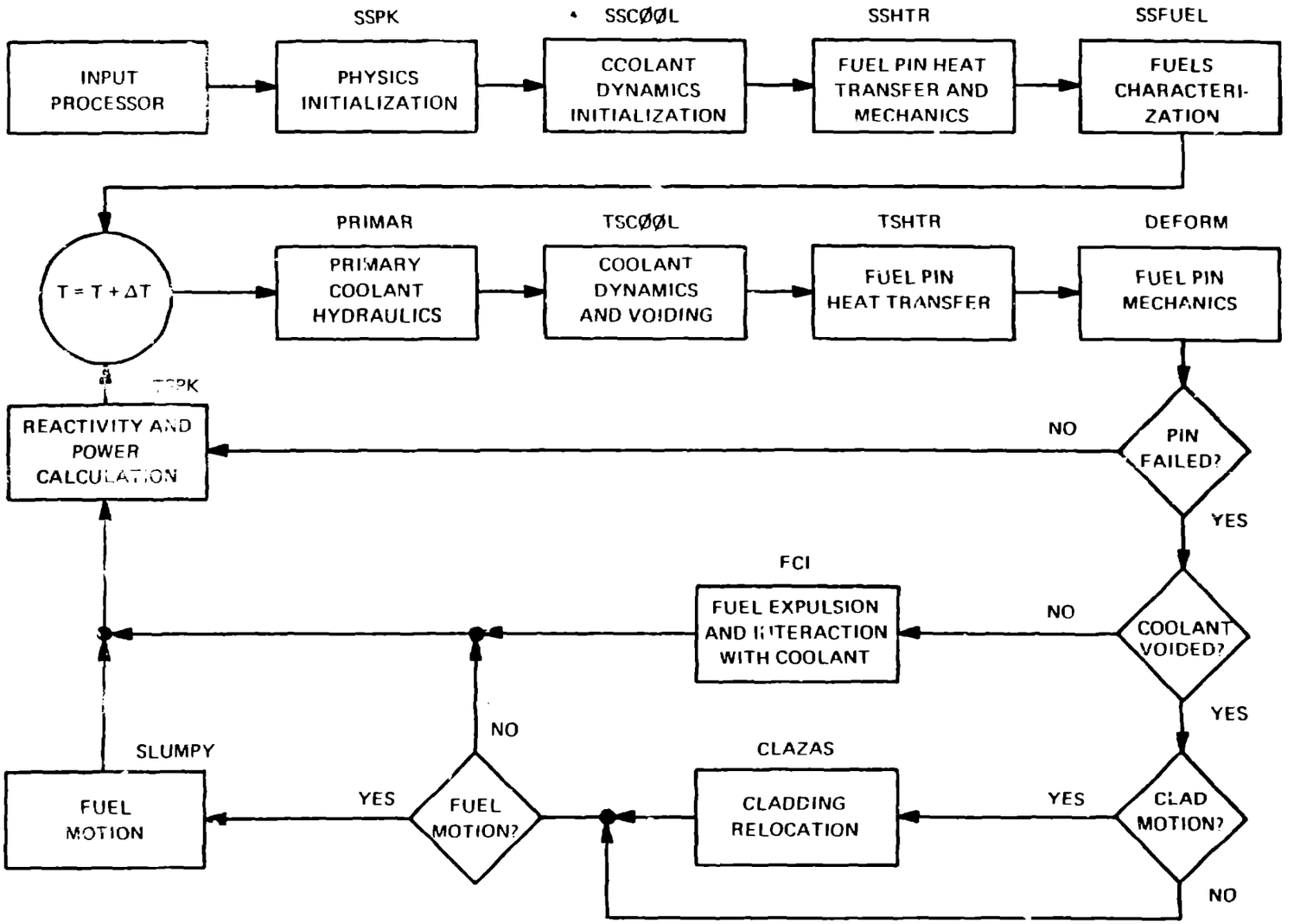
INPUT PROCESSOR
SSPK
PHYSICS INITIALIZATION
SSCØØL
CCOLANT DYNAMICS INITIALIZATION
SSHTR
FUEL PIN HEAT TRANSFER AND MECHANICS
SSFUEL
FUELS CHARACTERI-ZATION
T = T + ΔT
PRIMAR
PRIMARY COOLANT HYDRAULICS
TSCØØL
COOLANT DYNAMICS AND VOIDING
TSHTR
FUEL PIN HEAT TRANSFER
DEFORM
FUEL PIN MECHANICS
TSPK
REACTIVITY AND POWER CALCULATION
NO
PIN FAILED?
YES
FCI
FUEL EXPULSION AND INTERACTION WITH COOLANT
NO
COOLANT VOIDED?
YES
NO
SLUMPY
FUEL MOTION
YES
FUEL MOTION?
CLAZAS
CLADDING RELOCATION
YES
CLAD MOTION?
NO

3.1 Sodium Boiling

The sodium-boiling model used in SAS3A and SAS3D began as a new version of the single-bubble slug-boiling model included as an option in SAS1A. The new version was similar to the models of Cronenberg, et al.[45] and of Schlechtendahl[46] and included an explicit calculation of vaporization of a liquid film remaining on pins after voiding, of condensation in colder regions, and of vaporization or condensation on the liquid interfaces. This single-bubble model was appropriate for situations involving high superheat.

However, early calculations with superheats lower than 70°C showed that the lower liquid slug heated well beyond saturation, indicating that additional bubbles should form. This model then was modified to allow a new vapor bubble to form in the liquid coolant at any point where the liquid temperature exceeded the local time-dependent saturation temperature by more than the original superheat criterion. It also was observed that, because of the high rate of vapor production and the resulting vapor velocities, large axial pressure gradients should exist in a large vapor bubble. For this reason the model was modified to account for the pressure gradients and the resulting multibubble model was included in the standard version of SAS2A and in SAS3A. Figure 5 indicates the conceptual basis of the model. It allows the formation and continued presence of a number of bubbles in a channel and follows the bubbles either as they move up a channel and collapse (or reach the exit) or as they become sustained and void the channel.

One-dimensional Eulerian equations for the upper and lower liquid slug (or the whole channel before boiling starts) are written in the form,

$$\frac{\partial \rho_\ell}{\partial t} + \frac{\partial G}{\partial z} = 0 \ , \tag{1}$$

$$\frac{\partial G}{\partial t} + \frac{\partial}{\partial z}\left(\frac{G^2}{\rho_\ell}\right) = \frac{\partial \Gamma}{\partial z} - \rho_\ell g - \left(\frac{\partial p}{\partial z}\right)_f \ , \tag{2}$$

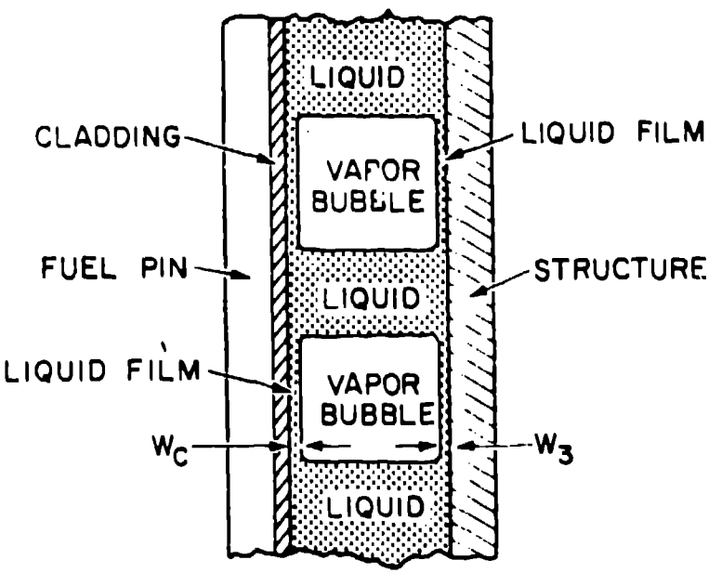

Fig. 5. Conceptualization of the SAS multibubble model.

where ρ_ℓ is the liquid density, G is the mass-flow rate, p is the pressure, g is the acceleration due to gravity, and $(\partial p/\partial z)_f$ is a friction pressure gradient. A lumped-parameter momentum equation for both upper and lower liquid slugs is obtained by integrating Eq. (2) over the length of the slug. The fixed grid used with the vapor region makes this something of a combined Eulerian-Lagrangian scheme.

For small bubbles, the pressure drop within the bubble is negligible and the bubble growth is determined by coupling the momentum equations for the liquid slugs with an energy and mass balance in the bubble, assuming saturation conditions and spatially uniform pressure and temperature. In the case of large bubbles, the voids can extend over regions with considerable axial surface temperature variation and the subsequent vaporization and condensation can cause high vapor velocities. This acceleration and the frictional effects are accounted for in an axially varying vapor pressure model. In this model, the vapor pressure, temperatures, and mass-flow rates are calculated at fixed nodes within the bubble and also at the lower and upper interfaces. This uses a simultaneous solution of the vapor cells momentum and continuity equations with the momentum equations for the liquid slugs setting the boundary conditions at the interfaces. Heat flow through the liquid-vapor interface is ignored in this model and the vapor velocity at the interface is assumed equal to the interface velocity. In addition, the pressures across this interface are considered continuous.

The SAS2A model accounted only for film dryout by vaporization, but for SAS3A a moving film treatment was added to account for film stripping by vapor shear. The frictional pressure drop in the vapor is increased due to the formation of waves or instabilities on the surfaces of the films. This is accounted for by using a vapor friction factor, f_v, in the form

$$f_v = f_o \left[1 + \frac{300\, M_f (W_c + \gamma_2 W_3)}{D_h (1 + \gamma_2)} \right] , \tag{3}$$

where

f_o = single-phase friction factor,

W_c = liquid film thickness on cladding,

W_3 = liquid film thickness on structure,

$\gamma_2 = \dfrac{\text{surface area of structure}}{\text{surface area of cladding}}$,

D_h = hydraulic diameter, and

M_f = user-supplied multiplication factor.

The resulting large shear force on the liquid film tends to lead to early local dryouts.

To obtain numerical stability for reasonably large time steps, an implicit differencing scheme is used, with the resultant simultaneous set of equations solved by Gaussian elimination. Time-step control is used when vapor pressures in any cell increase by more than 10% during a cycle. The reduced time step, Δt, is calculated from the original time step, Δt_o and the fractional increase in pressure, $\Delta p/p$, by

$$\Delta t_n = 0.075 \; t_o \frac{p}{|\Delta p|} . \tag{4}$$

The above procedure gives good results while allowing sufficiently large time-step sizes to render the calculations economically feasible. Overall, the SAS3A sodium boiling model has provided a reliable solution technique, particularly for loss-of-flow conditions, which has proven to stand well in comparison with numerous in-pile LOF experiments, such as in Refs. 47-49.

The basic aspects of the model are being retained for SAS4A, but refinements are being made, as discussed in Ref. 50, to extend its range of validity and to provide a more sophisticated solution technique. The new SAS4A model (1) accounts rigorously for the coexistence of sodium vapor and fission gas in voided regions; (2) allows heat transfer from dried-out cladding to the sodium vapor/fission gas mixture and superheating of the vapor; and (3) accounts for both spatial and temporal flow area changes, including those given by the cladding motion model. The numerical method used to solve the vapor conservation equations is a multicomponent generalization of the original Implicit Continuous Eulerian method.[51] As in the SAS3A moving film model, the vapor is coupled to the moving liquid sodium film on the cladding as long as the film remains. Both models essentially provide a two-velocity field (vapor and liquid) treatment for an annular flow regime. A comparison of the models for a calculation of a TREAT LOF test is given in Figs. 6 and 7. Despite variations in voiding profile oscillations, the overall behavior is very similar.

3.2 Cladding Relocation

In analyzing an unprotected loss-of-flow accident[52] for FFTF it was recognized that, under the expected relatively constant power conditions (the FFTF sodium void reactivity effect is small), cladding would melt some 2-3 s before fuel melting in the subassemblies that first voided. Thus, although there was no direct experimental evidence of such an effect, it was reasonable to assume that the molten cladding would relocate (possibly moving out of the heated region), freeze, and plug. The first supposition was that the cladding would drain downward and plug below the fuel region. However, following a suggestion by Fauske[53] it was recognized that upward sodium velocities could be high enough to cause flooding (wave formation), and the resulting high friction drag would lead to upward cladding motion similar to the sodium-film stripping effect included in the SAS voiding model. This could then lead to cladding freezing and an initial plug formation above the fuel region, followed by draining and plugging below the fuel region from cladding that melted later.

In addition to the mechanical effect on sodium voiding and fuel dispersal, cladding relocation can have a significant reactivity effect and a significant thermal effect in that removal of the cladding heat sink allows fuel temperatures to rise more rapidly. To analyze cladding relocation, the CLAZAS module[39] was developed for inclusion in SAS3A.

This model uses an explicit calculation of the motion of molten clad driven by the sodium-vapor pressure gradient and frictional drag. The physical picture is one of discrete clad segments that can combine by moving over other clad segments. Each segment moves under the forces of gravity, the channel pressure gradient, the frictional drag due to streaming sodium vapor, and the friction between moving clad and the fuel pin. Feedback effects are included to modify the coolant-channel sodium-vapor friction, the coolant channel hydraulic diameter, and the sodium-vapor flow area. Heat-transfer effects are calculated by including relationships describing the heat transfer from moving clad to stationary clad and from stationary fuel to moving clad, as well as a variable viscosity model for molten clad as a function of internal energy. Cladding

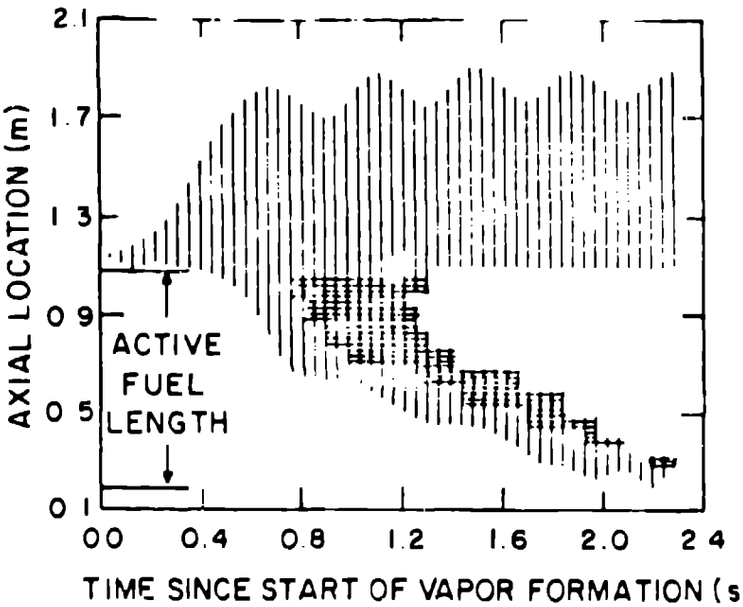

Fig. 6. SAS3D voiding, dryout, and clad melting pattern in a typical TREAT LOF test.

freezing is treated by increasing the cladding viscosity to a high value as the cladding internal energy decreases through the heat of fusion.

As an example, Fig. 8 shows an early CLAZAS calculation of the TREAT L2 experiment. This calculation was the first to indicate the suspected, but not previously observed, possibility of upper cladding blockage formation. It was a relatively successful example of ad hoc modeling, as the postmortem examinations did indeed indicate upper blockage formation.

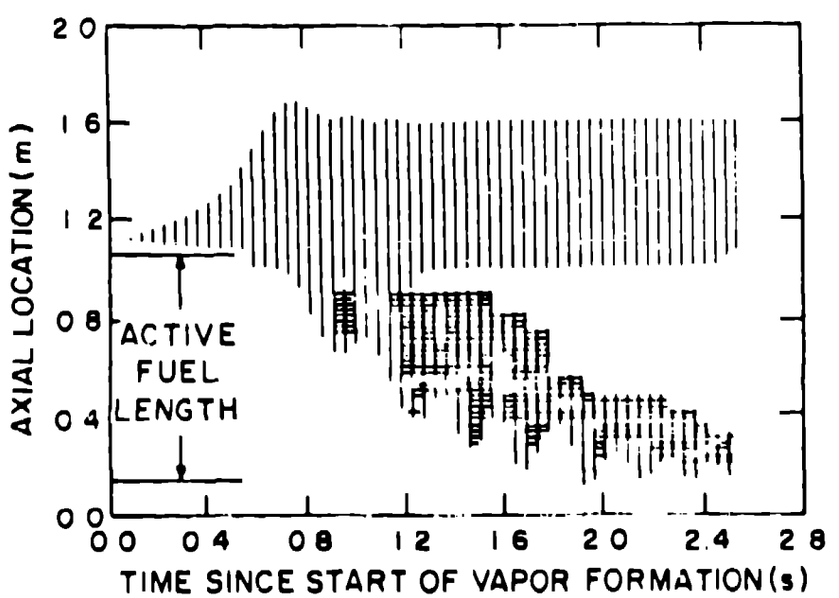

Fig. 7. SAS4A voiding, dryout, and clad melting pattern for the same problem shown in Fig. 6.

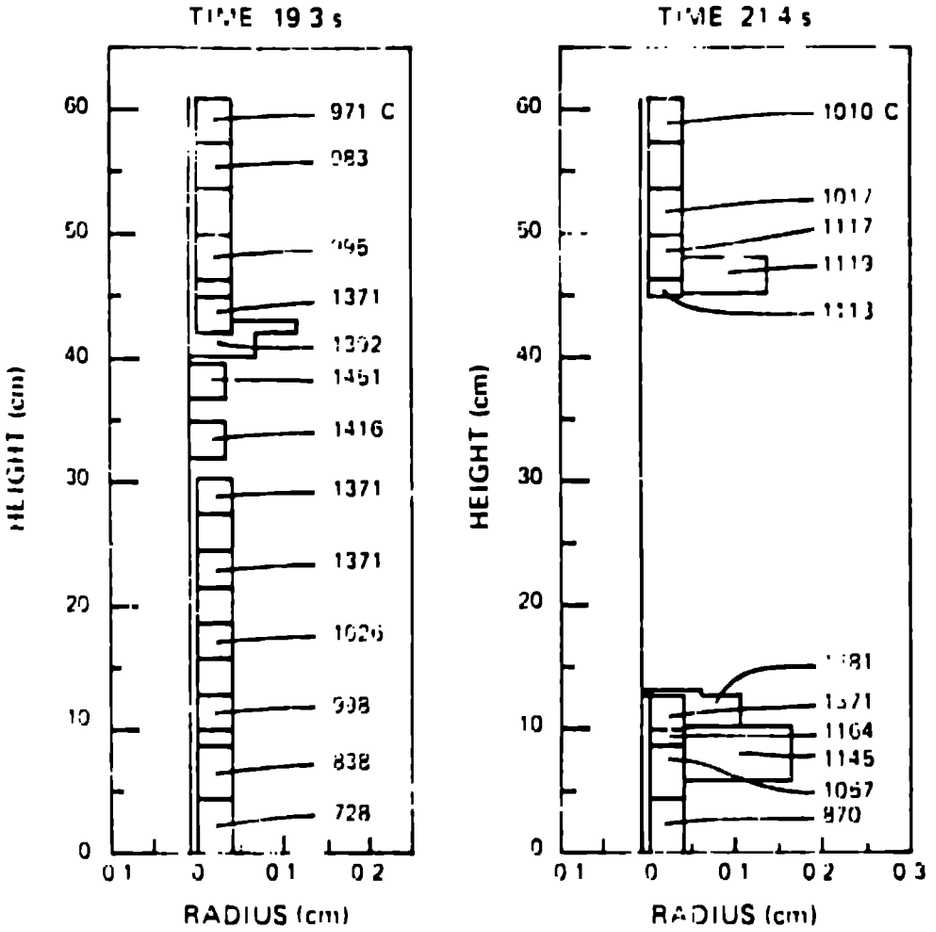

Fig. 8. CLAZAS calculation of L2 TREAT experiment showing cladding blockage at top and bottom of fuel column.

An improved model, CLAP,[42] was developed after CLAZAS and is being included in SAS4A. CLAP uses an Eulerian formulation rather than the Lagrangian-style cladding segments used in CLAZAS. Its predictions of smaller upper cladding blockages as compared to CLAZAS are in better agreement[54] with the observations from the more prototypic R-series TREAT LOF experiments.

3.3 Fuel Motion in Voided Subassemblies

A common and quite reasonable assumption in many fast reactor accident analyses has been that fuel, driven only by gravity, slumps as it melts. This was the basic assumption of the early Bethe-Tait analysis,[1] which assumed whole-core uniform slumping under gravity to provide a conservative bound for reactivity insertion rate. Gopinath and Dickerman[55] developed early slumping noncoherence arguments based on radial power distributions for EBR-II HCDA analyses. Because the mechanistic multichannel codes include this noncoherence effect directly, the emphasis during the last decade has been on including the several forces other than gravity that can act on fuel as it becomes mobile, either before or after initiation of melting. These forces include sodium vapor pressure gradients and shear, fission product pressures, and steel and fuel vapor pressures. The SLUMPY module[41] in SAS3A and SAS3D was the first

mechanistic model to include all these effects, albeit still in a somewhat parametric fashion.

SLUMPY provides a one-dimensional compressible-hydrodynamics calculation and can be used either to supply detailed initial conditions to a VENUS-II or other two-dimensional disassembly calculation, or it can be used directly as a disassembly code within the limitation of one-dimensional motion (implying intact subassembly geometry). In most SLUMPY calculations, fuel motion is assumed to be initiated when melting begins in unrestructured fuel.

As the fuel melts, individual axial fuel segments join the "slumped" region treated in the SLUMPY calculation shown in Fig. 9. Unmelted fuel above the slumped region can fall into or be pushed out of this slumped region. The unmelted pin below the slumped region is assumed stationary. Both the upper and lower solid fuel segments restrict the area available for the slumped region. Axially limiting boundaries for the slumped region are dependent on user input; or if CLAZAS is used, the boundaries may be determined by the time-dependent positions of calculated clad blockages.

Figure 10 shows a SLUMPY calculation of the TREAT L4 experiment. This early calculation shows "eructations" of fuel similar to those indicated by TREAT hodoscope measurements. In this SLUMPY calculation, the imposed heat-transfer assumptions led to these eructations being induced by steel-vapor pressures. Whether this or other mechanisms such as fission gas release cause such observed fuel dispersal events is still a subject of much discussion (a good review of fission gas effects is given by Deitrich in Ref. 56). SLUMPY provides a framework for including several mechanisms, with the notable exceptions that treatment of massive fuel swelling prior to melting or a "chunk breakup" mode of fuel disruption is difficult.

One of the necessary aspects of HCDA hydrodynamic models is that continued energy generation by fission and subsequent material vaporization provides a continued internal driving pressure for the momentum equations. In addition

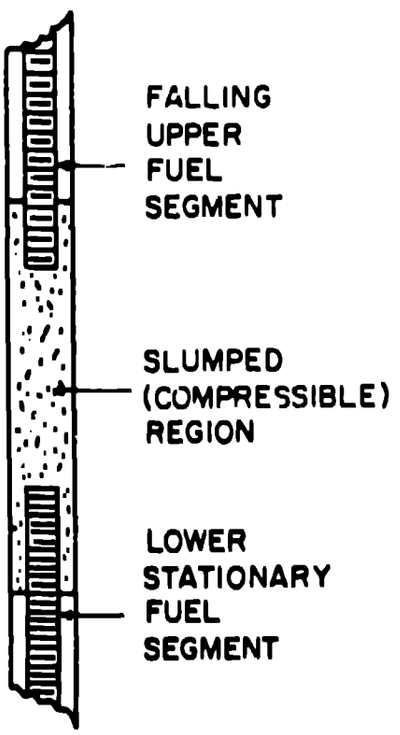

Fig. 9. Radially enlarged geometry showing fuel motion in a SLUMPY calculation.

Fig. 19. SIMMY calculation of LA TREAT experiment showing eructation induced by steel-vapor pressure.

to solving the conservation equations for a multicomponent system, the rate of energy generation and its transfer among the several possible components must be explicitly accounted for, with a feedback to the pressure field in the momentum equation through the equation of state. The SIMMY equation of state includes steel (iron) and fuel (UO_2) vapor pressure and uses fission gas or sodium vapor pressure as a background pressure when steel and fuel vapor pressures are low. Liquid compressibility is included when single-phase conditions are reached.

SIMMY was the first multicomponent HCDA analysis model to account for both separate velocity and energy fields with momentum and heat transfer between the fields. Several assumptions concerning viscous and friction effects, drag forces in a suspension, and heat transfer to the structure were employed to provide a sufficient number of equations for numerical solution. Slip is allowed between fuel particles and fission gas, but two-phase steel/fuel-vapor mixtures are treated as homogeneous flow. For the first case, a noteworthy simplification is that the fission gas inertial term is neglected; that is, the fission gas momentum equation is treated in a quasi-steady-state fashion.

The initial solution technique used in SIMMY was an Eulerian formulation with explicit time-differencing; but as is generally true for Eulerian methods (unless special techniques are used), definition of material interfaces proved difficult. Also, a severe numerical stability problem arose in regions of high-power density undergoing rapid fuel vapor expansions. For such reasons, the Eulerian approach was abandoned and an explicit Lagrangian approach with mesh rezoning was employed. Rezoning in SIMMY takes place when an additional fuel node satisfies an initiation-of-motion criterion. If material rapidly vaporizes and the mesh cell grows, the pressure gradient is spread over a fairly

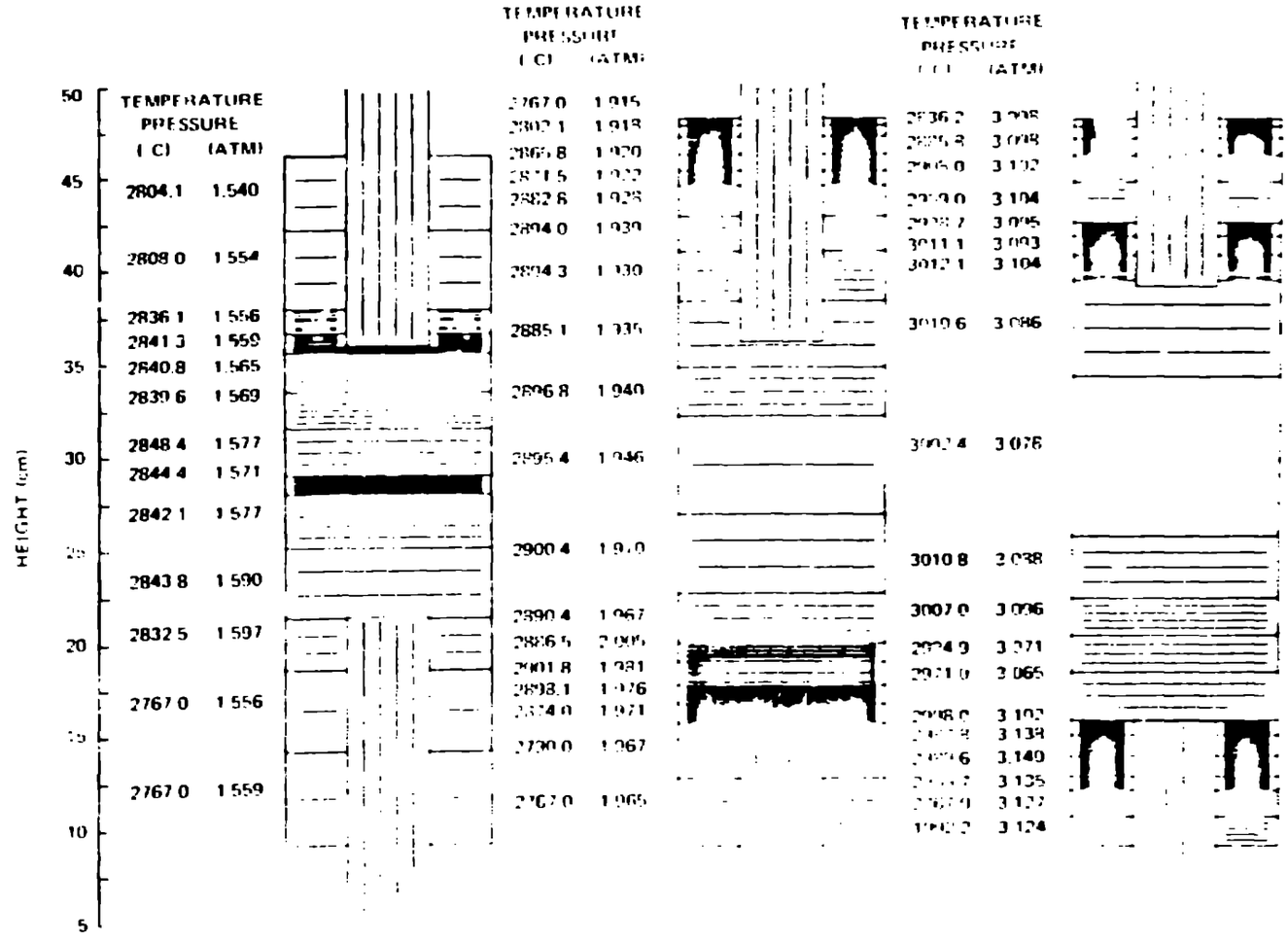
HEIGHT (cm)
50
45
40
35
30
25
20
15
10
5
TEMPERATURE
PRESSURE
(C) (ATM)
2804.1 1.540
2808 0 1 554
2836 1 1 556
2841 3 1 559
2640.8 1.565
2839 6 1 569
2848 4 1 577
2844 4 1 571
2842 1 1 577
2843 8 1 590
2832 5 1 597
2767 0 1 556
2767 0 1 559
TEMPERATURE
PRESSURE
(C) (ATM)
2767 0 1 915
2802 1 1 918
2865 8 1 920
2871 5 1 922
2882 6 1 925
2894 0 1 930
2894 3 1 930
2885 1 1 935
2896 8 1 940
2895 4 1 946
2900 4 1 960
2890 4 1 967
2886 5 2 005
2901 8 1 981
2893 1 1 976
2874 0 1 971
2730 0 1 967
2767 0 1 965
TEMPERATURE
PRESSURE
(C) (ATM)
2836 2 3 098
2865 8 3 098
2865 0 3 102
2893 0 3 104
2838 7 3 095
3011 1 3 093
3012 1 3 104
3010 6 3 086
3002 4 3 076
3010 8 3 088
3007 0 3 096
2924 9 3 071
2931 0 3 065
2998 0 3 102
2 3 138
2 6 3 140
2 7 3 135
2 4 3 122
2 2 3 124

large region. If rezoning then is performed using constant intervals, the pressure gradient at the top and bottom of the cell is increased substantially, causing rapid acceleration and compression of slower moving cells. This problem was resolved by performing the rezone so that cells have a certain minimum mass, instead of a minimum length. When the grid-mesh is rezoned, the field variables are transformed by a linear interpolation between the old and new mesh structure.

The minimum mass requirement also is significant in time-step control, which is based on a Courant condition.[57] When a cell with a small amount of vapor is compressed, the volume (or linear dimension in this one-dimensional formulation) is reduced substantially until single-phase conditions are reached. Thus, the denominator of the Courant number (the spatial mesh) is reduced significantly, requiring a compensating time-step reduction to ensure stability.

SLUMPY is being replaced for SAS4A with the LEVITATE model,[44] which provides a more consistently integrated treatment of fuel, steel, sodium, and fission gas dynamics in voided or nearly voided regions of channels. LEVITATE treats fuel motion inside disrupting pins and, as a pin becomes completely disrupted, the channel treatment includes three velocity fields (a liquid fuel and steel field, a solid fuel fragment or chunk field, and a mixed vapor field) in an Eulerian grid. The solution technique is explicit in time and is coupled integrally to the liquid sodium slug calculation in the channel. LEVITATE, through including various fuel breakup modes, several flow regimes, cladding and structure ablation, fuel-steel mixing, and fuel-steel mixture freezing, removes most of the modeling limitations of SLUMPY. Because of its similar explicit numerical treatment, however, it is not likely to decrease computing times significantly.

3.4 Fuel Pin Failures

Several possible modes of fuel pin failure (i.e., cladding failure) can occur during a disruptive accident. Some are relatively simple to predict, such as cladding rupture due to plenum fission gas failure or cladding melting following dryout during sodium boiling. However, the prediction of cladding rupture during an unprotected transient overpower accident is more difficult and has been the subject of considerable modeling and experimental effort. A central problem has been whether fuel-cladding relative thermal expansion or transient fission gas release from the fuel and internal pressurization is the major contributor to cladding damage and failure.

A straightforward analysis of relative thermal expansion, assuming elastic fuel and elastic-plastic cladding, was included in the DEFORM-I model of SAS1A. DEFORM-II in SAS2A, and as an option in SAS3A, provided a similar analysis but included an elastic-plastic fuel treatment and allowed treatment of a central void and transient fission gas release. However, it did not allow for radial cracking of the outer part of the fuel pellets and the resulting loss of strength, particularly important when high pressures from fission gas release, fuel expansion on melting, and fuel vapor pressure occur in the fuel central region. Also, a reliable high-temperature failure criterion based on plastic deformation was not available during the time SAS3A was developed.

For these reasons, a "burst pressure" failure was included in SAS/FCI. This assumed pin internal pressures could be transmitted directly to the cladding (with a 1/r loss) through radially cracked and strengthless fuel. Unlike the thermal expansion loading mode in which cladding strain relieves the loading, the loadings caused by transient fission gas pressurization are not

sufficiently relieved by local cladding deformations. Thus, an ultimate strength failure criterion (the burst pressure) rather than a strain failure criterion was used in SAS/FCI.

Both DEFORM-II and the burst pressure criterion model in SAS/FCI have serious limitations, and several models have been developed that remove these limitations. One of the first of these is LAFM[53] which uses a cladding life-fraction damage correlation to predict failure and has been verified by comparison to a large number of TREAT TOP experiments. LAFM calculations have indicated that depending on transient conditions, either thermal expansion, fission gas release, or a combination can be the cause of failure. A similar model, DEFORM-III [50] has been developed for inclusion in SAS4A.

3.5 Fuel Motion/FCI in Unvoided Channels

Early analyses[60] of a mild overpower transient HCDA in FFTF assumed that if the fuel pins failed at the midplane, plenum fission gas release through the failure could cause rapid voiding, leading to a prompt-critical transient and core disassembly. This mechanism was recognized to be unrealistic, and later modeling concentrated on developing a more consistent scenario for the phenomena following fuel-pin failure. The FISFAX model[61] was used to evaluate a sodium-in prompt-critical transient in FFTF and was the first to include the effect of sodium-induced fuel-coolant interaction (FCI) dispersive fuel motion. This concept, along with more realistic estimates of fuel-failure locations, went into the models used in later FFTF analyses. These analyses indicated that a hydraulic fuel-sweepout mechanism could terminate mild reactivity transients well before prompt criticality was reached.[33] Calculations with the SAS/FCI module[40] in SAS3A also indicated early termination, although in both cases the modeling originally was developed to provide a realistic estimate of the reactivity insertion rates as initial conditions for core-disassembly calculations rather than to predict early accident termination.

SAS/FCI is essentially a "point" or lumped parameter model as opposed to the one-dimensional voiding, cladding motion, and fuel motion models in SAS3A. SAS/FCI integrates the effects of fuel/fission gas mixture expulsion into flowing liquid sodium, the thermal interaction between molten fuel and sodium (based on a Cho-Wright parametric model[24]), condensation of sodium vapor (noted to be important in an early analysis of Cronenberg[62]), sodium slug ejection, and the resulting sodium and fuel motion reactivity effects. Cladding failure time and location can be set by input criteria using fuel thermal conditions, although SAS/FCI also includes the internal pin pressure failure criterion noted above. Although the fundamental modeling employs a lumped-parameter treatment for temperature, pressure, and sodium density in the interaction zone, a pseudo-Lagrangian model is used to treat fuel motion. In this model, the fuel moves with a velocity found by linear interpolation of the interface velocities of the two constraining liquid sodium slugs. Fuel motion inside the pin is treated by assuming a uniform decrease in density. It can be easily envisioned that this overpredicts the positive reactivity effect of internal motion if the failure is at the core axial midplane. Conversely, negative reactivities are overpredicted with away-from-midplane failures.

The numerical method of SAS/FCI uses explicit time-differencing of a single ordinary differential equation describing the interaction-zone pressure. This single equation was derived analytically from the momentum equations that couple pin internal and coolant channel pressures and the FCI zone internal energies. Back substitution is used to obtain other dependent variables.

Although small time steps generally are required, the method still is quite efficient.

When pin failures and fuel-coolant interactions occur as calculated by SAS/FCI, resulting high pressures in the coolant channels are felt instantaneously in the inlet plenum (the liquid slugs are assumed incompressible). Rapid inlet pressurizations can be calculated, particularly when many subassemblies are in the channel undergoing the FCI process. This pressurization tends to increase flows in other channels and to delay heatup. Although it is unrealistic to include this coherence enforced by lumping many subassemblies together and assuming that all pins fail simultaneously, the possible importance of this effect led to the treatment of primary loop pressures and flow rates included in the PRIMAR-II module[63] of SAS3A, and more recently, PRIMAR-IV in SAS4A.[64]

A primary limitation of SAS/FCI has been its inability to treat fuel expulsion into partially voided regions of a channel, as is typical of some channels in an ULOF overpower condition (the LOF/TOP syndrome). This limitation and its unrealistic predictions of fuel motion reactivities have led to development of the one-dimensional codes PLUTO[65] (a Lagrangian code), PLUTO2[43] (Eulerian), and EPIC[66] (Eulerian, Particle-in-Cell). Both PLUTO2 and EPIC have been or are being coupled to a version of SAS (EPIC in SAS3D and PLUTO2 to be in SAS4A). Figure 11 shows a comparison of SAS/FCI and PLUTO2 calculations of the TREAT L3 experiment from Ref. 5.

These models provide the only available mechanistic treatment of what is termed as loss-of-flow-driven transient-overpower (LOF/TOP) conditions. If, in a loss-of-flow accident, voiding, cladding relocation, and/or fuel slumping do lead to a sufficiently high overpower (TOP) condition, pins in colder subassemblies can fail with fuel expulsion into liquid sodium. If large positive reactivities result following near midplane failures, autocatalytic behavior can be calculated, i.e., the high-power levels cause more rapid pin failures, inducing higher insertion rates, higher power levels, and even more rapid pin failures (SAS/FCI overpredicts this effect). PLUTO2 predicts[67] that such autocatalytic behavior is much less likely than given by SAS/FCI predictions.

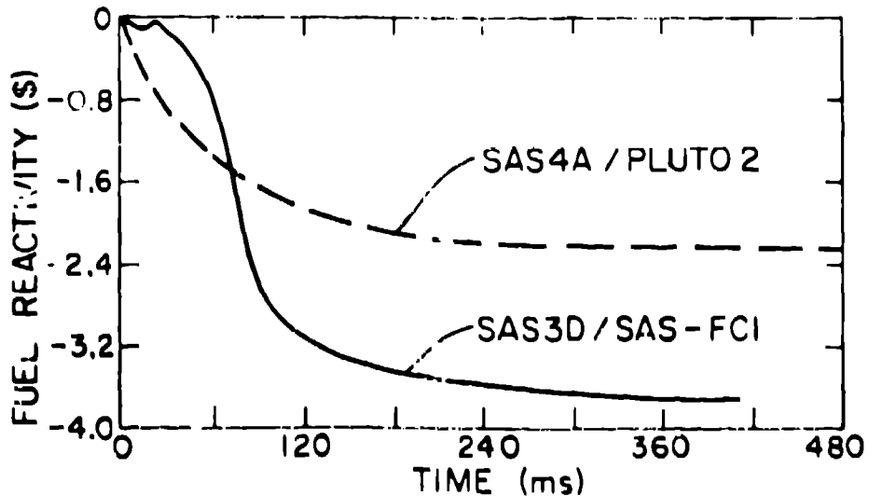

Fig. 11. Comparison of SAS/FCI and PLUTO2 postfailure fuel reactivity feedback calculations.

4. DISASSEMBLY MODELS -- VENUS-II

Numerous hydrodynamic disassembly models have been developed. They all share the basic approach, first proposed by Bethe and Tait,[1] of treating the core materials as a hydrodynamic fluid. Early models also assumed that the material densities remained constant during disassembly to facilitate analytical solutions of the equations.

The first model to provide a direct numerical solution to the multidimensional hydrodynamics equations was the VENUS[6] code developed at Argonne National Laboratory (ANL). This represented a significant advance in capability because the inclusion of an explicit calculation of the material density changes allowed the use of a more accurate density-dependent equation of state. The current version of this code, VENUS-II,[7] will be discussed as an example of the techniques in the disassembly area.

The hydrodynamics equations are solved in r-z Lagrangian coordinates. Because the grid mesh deforms with the material, mass conservation is merely expressed by

$$\rho = \frac{\rho_o V_o}{V_t} , \tag{5}$$

where ρ and V_t are the density and total volume of the mesh cell and ρ_o and V_o are the initial values.

The radial and axial accelerations of each mesh point are calculated from the momentum equations

$$\ddot{r} = -\frac{1}{\rho}\frac{\partial p}{\partial r} \qquad \text{and} \qquad \ddot{z} = \frac{1}{\rho}\frac{\partial p}{\partial z} , \tag{6}$$

where r and z are the Eulerian coordinates of a given point in the Lagrangian grid mesh. The pressure, p, is the sum of the pressure obtained from the equation of state and the Von Neumann-Richtmyer viscous pressure.

The momentum equations are solved with an explicit, first-order, finite-difference technique previously used in hydrodynamics codes developed at LASL[27] and in the REXCO damage evaluation codes to be discussed later. In this approach, the positions, velocities, and accelerations are associated with the mesh points, while such quantities as the pressures, densities, and internal energies are associated with the mesh cell centers. A detailed development of the finite-difference equations and solution strategy is presented in Appendix B.

As with any explicit numerical calculation, the time-step size must be controlled properly to ensure a stable and accurate solution. The requirements on the time-step control are made especially stringent because of the density-dependent equation of state used. When single-phase conditions develop in a mesh cell, the resulting pressure is an extremely sensitive function of the internal energy and density.

The influence on the time-step size can be appreciated by considering a time step during which a cell being compressed passes from two-phase to single-phase conditions. As soon as the cell volume is decreased to the point where all the vapor space is eliminated, a large resisting pressure should start

developing. Because finite time steps must be used, the usual situation is to reduce the volume somewhat beyond this point. This causes the compression to be overestimated. If the time steps are too large, the resulting pressure in the compressed cell can then be greatly overestimated.

The VENUS-II time-step size is controlled using the stability index

$$w = \frac{c^2}{A}\left(\frac{\Delta t}{1.2}\right)^2 + 4\left|\frac{\Delta V}{V}\right| , \qquad (7)$$

where c is the speed of sound, A the mesh cell area, V the specific volume, and ΔV is the change in the specific volume during the time step. The time-step size, Δt, is adjusted to keep the maximum value of w for all mesh cells within empirically determined limits.

In general, the time-step size must be kept very small (< 10 μs) whenever single-phase conditions are encountered. This does not seriously restrict the analysis of energetic excursions, as the time scales that must be covered are of only a few milliseconds. Fairly long running times are required for mild excursions that involve extended single-phase pressure conditions, however.

A significant limitation of a two-dimensional Lagrangian disassembly model, like VENUS-II, arises because it cannot easily calculate large material displacements. The model becomes inaccurate and eventually unstable when the distortions of the grid mesh grow too large. This restriction is not important in analyzing an initial energetic burst because the power excursion is normally terminated by a relatively small outward displacement of the fuel. Only a few centimeters of displacement occur before the power has decreased to insignificant levels. Although the Lagrangian calculations can be extended to larger displacements using rezoning techniques (this is done in some REXCO calculations), numerous other complications, such as the interaction of the expanding core materials with the surrounding structure, must then be considered.

5. NEUTRONICS

While far more effort has gone into refining numerical methods for steady-state neutronics analysis of fast reactors, neutron kinetics also has been an area of considerable interest. Most fast-reactor accident codes have used point kinetics (in particular, SAS3A and VENUS-II); but more recently, multidimensional kinetics methods are coming into wider use.

As is well known, when material density changes and the resulting flux shape and spectrum changes are small, first-order perturbation theory and point model kinetics are adequate. Generally, point kinetics is sufficiently accurate to predict neutronics behavior during initiating-phase events before substantial fuel motion. Similarly, in a classical core disassembly, large negative reactivities and neutronic shutdown result from relatively small outward motions and, again, perturbation theory and point kinetics are sufficiently accurate (as was assumed in the original Bethe-Tait analysis). Some space-dependent effects and differences in diffusion and transport theory can be found even in the two cases noted, but more important effects occur with the large fuel motions typical of large-scale fuel slumping or dispersal in the initiating phase and of the gross fuel motions occurring in the transition phase.

Two approaches have been taken in adding space-dependent kinetics to fast-reactor accident analysis codes. For one, direct finite-difference methods have

been developed (e.g., one based on an explicit exponential extrapolation method to solve the two-dimensional multigroup time-dependent transport equations was included in SIMMER-I). The second approach began with the "improved quasistatic" method of Ott and Meneley[69] and provided the first two-dimensional time-dependent multigroup diffusion equation solution used for fast-reactor accident analysis. This method was used in the FX2 code,[70] which was coupled to the original VENUS code.[71] This particular combination was not very useful because the small displacements allowed by the VENUS Lagrangian treatment did not lead to significant space-dependent neutronics effects.

The quasistatic method factors the space-, energy-, and time-dependent flux (and angular-dependent in the case of transport theory) into a gradually developing time-dependent spatial flux shape and an amplitude function, that is,

$$\phi(x,E,t) = \phi(x,E,t)\, T(t) .$$

This form is substituted into the appropriate diffusion or transport equation, is weighted (generally with the stationary adjoint flux), integrated over all independent variables except time, and is normalized on ϕ, such that

$$\iint \frac{\phi^*(x,E,0)\ \phi(x,E,t)}{v}\, dx dE = \text{constant} .$$

An ordinary differential equation for T(t) results. This equation has the form of the usual point kinetics equations and specifies how the basic parameters can be calculated from the spatial flux shapes. The flux shapes can be calculated with conventional steady-state flux methods with some source terms added.

Because this method makes maximum use of existing static flux shape calculational methods and because it requires a minimum of full space-dependent flux calculations, the improved quasistatic method has been adopted for both SAS4A (as a two- or three-dimensional multigroup diffusion theory solution) and in SIMMER-II (as either a multigroup diffusion or S_n transport theory two-dimensional solution). In recent applications of SIMMER-II, both full space-dependent kinetics and a transport theory treatment have proved necessary for certain transition phase problems.[72]

6. GENERAL CORE DISRUPTION AND EXTENDED MOTION -- SIMMER

The ultimate goal of the material motion analysis for a core-disruptive accident is to describe the fuel motion until a permanently subcritical and coolable configuration is attained. This provides initial conditions for damage evaluation and postaccident-heat-removal calculations. In many cases, this involves removing a sizable fraction of the fuel to a position well beyond the immediate core region. For accident sequences that do not proceed directly into a gross mechanical disassembly, this removal process may occur over many seconds and may involve complex interactions with the structure surrounding the core. Because such codes as SAS and VENUS-II were unable to address this problem properly, the development of several new models was instigated.

The limited Lagrangian methods led to the development of the extended material motion codes, such as TWOPOOL and VENUS-III at ANL and SIMMER at LASL. These are all based on the Implicit Continuous Eulerian (ICE) two-fluid method developed by Harlow and Amsden and used in the KACHINA code.[73] VENUS-III and TWOPOOL, with their emphasis on numerical efficiency, are very useful for a

class of problems. Because SIMMER-II has a broader range of applicability achieved by including a structure field and all core materials, it will be the subject of the further discussion here.

The SIMMER (S_n, Implicit, Multifield, Multicomponent, Eulerian, Reactivity) development effort was begun in 1974 to provide a general mechanistic code framework to address all the disruptive accident analysis events occurring between those covered by the multichannel codes, such as SAS, and the damage assessment codes such as REXCO. One of the initial objectives was to provide a tool for resolving questions of recriticality[74] following core material expulsion after a mild disassembly. However, the SIMMER modeling framework was made sufficiently general to allow studies of transition phase development.

SIMMER-II is a coupled space- and time-dependent neutronics and multiphase, multicomponent Eulerian fluid dynamics computer code designed to calculate the two-dimensional (r,z) motion of LMFBR core materials during a core-disruptive accident. The neutronics calculation in SIMMER-II employs the quasistatic method to solve either multigroup diffusion or transport equations in two space dimensions (r,z) and in time. As an option, the point kinetics equations may be solved. The fluid dynamics calculation solves multicomponent, multifield coupled equations for mass, momentum, and energy conservation. (A field is a set of materials having the same velocity distribution.) In SIMMER-II all vapor components have one velocity and all liquid components have another velocity at a given space-time point. The two fields are momentum-coupled through drag terms. In addition to the two moving fields, a "structure field" is included to account for still-intact solid materials. Mobile particulate solid material also is allowed in the "liquid" field.

Each velocity field contains several components, and each component is described by density and internal energy distributions. To account for different enrichment zones and different degrees of burnup, the fuel material in SIMMER-II can be separated into fertile and fissile components. For example, in an LMFBR fueled with mixed uranium and plutonium dioxide, the fertile component can be approximated as depleted uranium dioxide and the fissile component as plutonium dioxide. These two components are modeled by two distinct density distributions, but, because they are intimately mixed, only one energy distribution is necessary to determine their common local temperature. A control material component that usually is modeled as boron carbide (B_4C) is needed to treat the neutron absorption effect of this material and its thermal interactions with other materials in the reactor core. A fission gas component also is included, not only to provide pressure when it is released from the unrestructured fuel matrix to the vapor field, but also to account for the presence of noncondensibles in the phase transition models. Thus, SIMMER-II has six basic components: fertile fuel, fissile fuel, steel, sodium, control material, and fission gas. A separate accounting must be made of materials that melt and then freeze either as particulates in the liquid fuel or on still solid structural components (the can walls, for example).

Figure 12 summarizes the SIMMER computational and modeling framework. Within each fixed (Eulerian) grid mesh, considerable modeling detail is allowed through the multifield calculational technique; that is, liquid and vapor flow are treated with separate conservation equations and the structural field is used for solid elements (intact fuel, cladding and wire wraps, control rods, and subassembly can walls). Subassembly can walls, if intact, restrict radial motion between cells. In this way, the methodology can encompass a multichannel treatment as with an initiating-phase code such as SAS3A. Radial motion is allowed when can walls are calculated to fail as occurs in a transition phase.

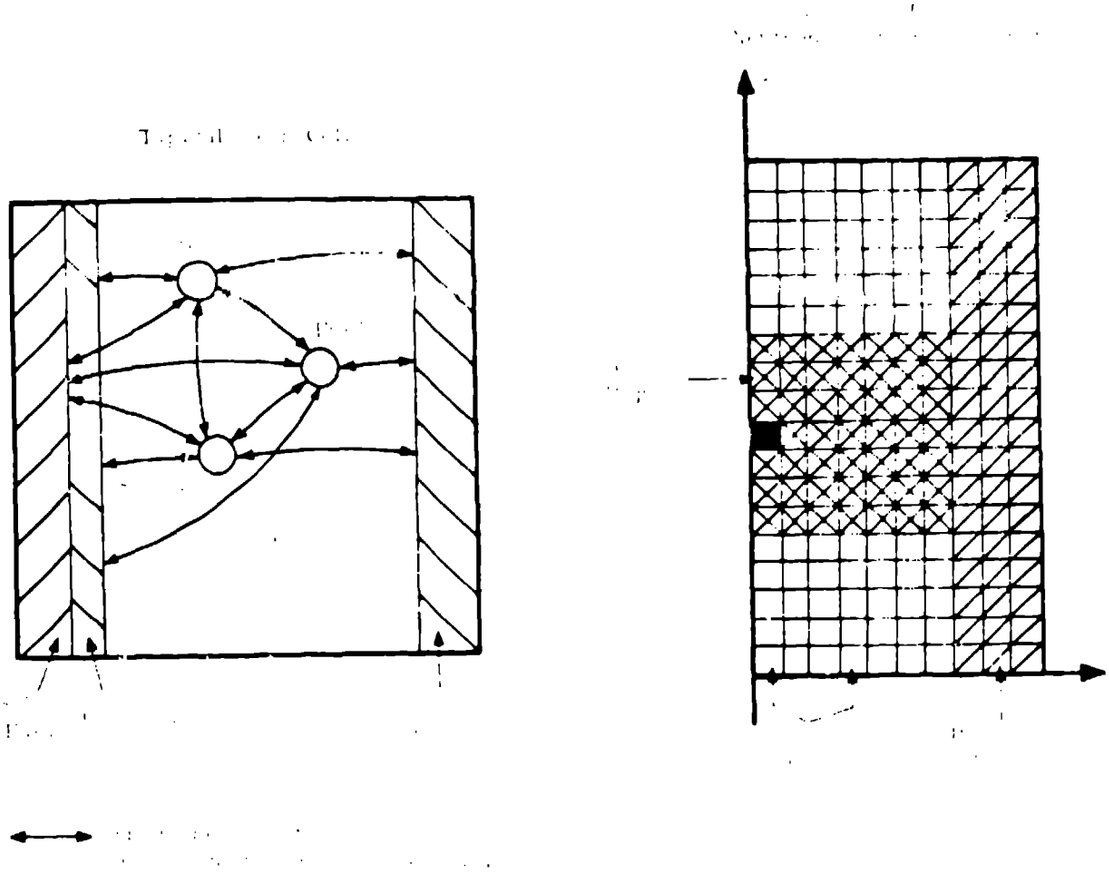

Fig. 12. SIMMER modeling framework.

This modeling framework allows the inclusion of energy and momentum exchange between almost any phase (solid, liquid, or vapor) of any component (represented only as sodium, steel, and fuel in Fig. 12) and another phase of the same component or any phase of another component. This is indicated in Fig. 12 by the arrows. The liquid phase is represented here by dispersed droplets in the continuous vapor field, which is a mixture of component vapors. The modeling framework also includes mass exchange between all phases of most components (obvious exceptions are that solid sodium and solid or liquid fission gas are not included). Thus, structural components, including fuel, cladding, and can wall steel, and control material can melt, begin to move, and eventually vaporize. Similarly, vapors can condense and liquids can freeze, all as dictated by heat-transfer processes and energy conservation.

The multicomponent field equations include numerous coefficients, generally as analytical functions, which model mass exchange, momentum exchange, and energy exchange among all the components. Usually, these are included in the form of generally accepted engineering correlations, such as heat transfer relations of the form

$$q_{ab} = h_{ab} A_{ab} (T_a - T_b) ,$$

where a and b could represent two phases of the same component (nonequilibrium is allowed), two components in the same phase (except that only one average vapor energy and temperature are used), or two components in two phases (such

7. CONTAINMENT EVALUATION METHODS

The Reactor EXcursion COntainment (REXCO) codes were developed to analyze the response of LMFBR primary systems to core-disruptive accidents. An early version of REXCO-H[75] provided only a two-dimensional hydrodynamics analysis. A later version, REXCO-HEP,[10] also included the elastic and plastic deformations of the reactor structures and components.

The equations of motion are treated with the same two-dimensional Lagrangian formulation discussed earlier for the VENUS-II code. A main difference is in the equation of state, as the REXCO codes deal principally with sodium as a working fluid. In addition, an Eulerian formulation was developed to facilitate the calculation of larger degrees of material motion. This code, ICECO,[76] also is based on the ICE[51] formulation. The convective terms in the mass equation and the pressure gradients in the momentum equation are evaluated at advanced times. Elimination of the mass-flux between the mass and momentum equations, in conjunction with an equation of state relating density and pressure, reduces this set to a Poisson-type equation.

A newly developed technique[77] for adapting ICECO to handle moving boundaries (which is straightforward with the Lagrangian codes) treats the reactor vessel boundary as a locus of nodal points as in REXCO-HEP. Movement of these points may be the result, for example, of fluid impact that deforms the vessel boundary. The movement of this Lagrangian boundary then is mapped onto the fixed Eulerian grid, providing the regions at which the hydrodynamic boundary conditions must be satisfied.

8. VERIFICATION OF WHOLE-CORE ANALYSIS CODES

The many models discussed above have been tested against experimental data using several different approaches. The SAS code has not been tested in its full form; instead, the separate models were compared to data from integral experiments performed with a few (1, 3, or 7) test pins in the TREAT reactor or with 19 and 37 test pins in the Sodium Loop Safety Facility (SLSF) loop in the Engineering Test Reactor. Generally, the goal has been to achieve reasonable qualitative agreement with the test data, particularly regarding cladding and fuel motion. For the sodium boiling model, quantitative agreement of voiding rate has been achieved both for out-of-pile tests in the OTPA loop and in-pile R-Series 7-pin tests in TREAT.[47] Agreement with 19-pin LOF tests in the SLSF loop in the ETR is also good.[48,49]

No time-dependent quantitative data are available for cladding relocation. However, the main objective of cladding relocation models is to predict the timing and location of blockage formation. As noted earlier, a reasonably successful test was achieved with the original CLAZAS model when it predicted upper cladding blockages in the TREAT I2 test. However, the CLAZAS model tended to overpredict upper blockage in the longer pin R-Series experiments. The newer CLAP model to be released in SAS4A predicts smaller upper blockages, in better agreement with the tests.[5]

Verification of SIMMY has been more difficult, as the only fuel motion data available are those from the fast neutron hodoscope at the TREAT reactor. SIMMY calculations have been tuned to fit the relatively rapid excursions of fuel observed by the hodoscope in a number of TREAT tests. The first example of this was the comparison noted earlier of a SIMMY calculation of the TREAT 1A experiment. In these calculations the cladding was assumed to remain on the fuel and was mixed with the fuel after motion was initiated. The heat-transfer

as liquid steel to solid intact fuel pellets). As is usual with such general relations, considerable care must go into the specific h, A, and ΔT quantities used. This is particularly true in the SIMMER framework, not only because of the many components treated, but also because these terms contain all the modeling information; for example, there is no standard geometry that fixes the interfacial areas. Even the structure field geometry and the resulting areas must be included through input parameters. This leads to some inconvenience in setting up analysis problems, but allows much more flexibility than fixed geometry models. As an example, a dispersed-droplet flow regime is the nominal regime used in SIMMER-II, but other flow regimes can be modeled by using appropriate exchange functions. The major limitation is that changes from one regime to another cannot be treated in a single calculation.

The SIMMER-II fluid dynamics numerical methods are based on those of the PAHTNA program, which was the first to use the implicit multifield method. The methods were extended considerably to treat the many components and more complex exchange process models included in SIMMER-II.

The field equations are differenced in space using a partial donor cell method. The full set of spatially differenced time-dependent equations is solved in three basic steps: (1) calculation of the intra-cell exchange functions and rates (most of the intra-cell rate equations are solved implicitly), (2) an explicit calculation of the spatially differenced continuity and energy equations and portions of the momentum equations, and (3) a complete implicit calculation of the continuity and momentum equations (except that momentum convection is treated explicitly), and the pressure (from the equation of state).

For two-phase cells, an important part of the first step is an implicit calculation of the liquid droplet size, based on several criteria including a local Weber number. The implicit iterative solution scheme couples the Weber number criterion, the liquid vapor drag correlation, and truncated versions of the momentum equations. This implicit scheme stabilizes the droplet size calculation. The single-size (for each component in each mesh cell) droplet restriction provides only a crude approximation to the complex flow topologies likely to occur, but the droplet size does yield an interfacial area dependent on the relative velocity between liquid and vapor, which is important to both the energy and momentum exchange processes. The phase transition rates, also dependent on droplet size, are also calculated partially in an implicit manner, although not in the pressure iteration involved in the third step of the fluid-dynamics solution.

Step two, the explicit part of the fluid dynamics calculation, provides a relatively straightforward first solution of the continuity and energy equations. The third step is similar to the pressure iteration used in PAHTNA although modified somewhat. An explicit step is taken on the momentum equations to calculate first-iteration advanced-time-step momentum fluxes. An iteration on the advanced-time pressure, density, and velocity distribution is made using the continuity and momentum equations and an equation of state (there are both analytical and tabular options included for the various equations of state needed). The momentum convection terms are included explicitly to avoid the full nonlinearity.

Numerous time-step controls exist in SIMMER-II, including those to account for rapid phase transitions. Because momentum convection is treated explicitly, a Courant limitation on material velocity (but not sound speed) results. That is, material cannot be convected more than one mesh in a single time step, but there is no similar restriction on pressure waves.

assumptions were such that steel vapor pressures began moving fuel at about the time of the observed eructation. In this case, the final configuration of the fuel was qualitatively similar to that observed in posttest neutron radiographs.

Despite some successes in fitting experimental data, the large uncertainties in the fuel breakup, fission gas release, and heat-transfer parameters in SLSYPY do not allow a unique set of parameters for reliable extrapolation to other test conditions. The new LEVITATE model, which is much more mechanistic than SLSYPY, is being tested against TREAT experiments and may permit such extrapolations. Significant data base uncertainties still exist in defining timing and modes of fuel pellet breakup and of fission gas release, however.

SIMMER code verification has proceeded with a completely different approach. Because no reactor material tests are available on relevant SIMMER regimes, many simulant materials tests have been analyzed. As noted earlier, the SIMMER calculational formalism is different from that of codes like SAS. SIMMER solves the conservation equations at each mesh cell at every time step. There are no special subroutines for computing specific phenomena; for example, the equation set used to compute heat transfer from a fuel pin to liquid sodium in a channel also is used to compute liquid-fuel to liquid-sodium heat transfer. Only the exchange coefficients vary. Because no specialized subroutines compute such things as freezing, vaporization, cladding motion, fuel motion, or fuel-coolant interactions, SIMMER verification rests principally on proper representation of the exchange functions (heat transfer and drag coefficients, for example). These exchange functions are obtained from engineering correlations that are applicable only over specific limited ranges; thus SIMMER can best be verified only over these specific ranges. This conclusion has led to testing SIMMER only for specific accident problems.

The initial SIMMER verification effort has been on extended expansions resulting from postulated core disassemblies. This emphasis came about from the SIMMER results[5] indicating that the system kinetic energy following a prompt-critical burst in the CRBR would be reduced many fold from an ideal isentropic expansion. For example, in CRBR, a kinetic energy of about 100 MJ is associated with an isentropic expansion to the cover-gas volume following a voided-core disassembly driven by about a $75/s prompt rate. SIMMER calculates a system kinetic energy at the cover-gas volume of about 5 MJ. This dramatic reduction in kinetic energy is caused by both fluid dynamics effects and rate-controlled phenomena.

SIMMER-II was used to analyze scale expansion experiments performed at the Stanford Research Institute (SRI)[79] to test its ability to calculate the hydrodynamics of bubble expansions. After some minor numerical method modifications, SIMMER-II predicted the experimental results with excellent accuracy.[80] Similar analyses of Purdue University CSTA nitrogen bubble expansion experiments[81] and of CSTA experiments[82] show good agreement except that shock fronts from high pressure (about 100 MPa and higher) expansions in the CSTA experiments are smeared by the SIMMER Eulerian hydrodynamics formulation.

SIMMER also has been used to investigate rather fundamental fluid dynamics problems including single-phase shock propagation, entrance-length effects in laminar flow, and steady laminar flow. (These results have been documented in Ref. 83.) In general, the results of these basic physics calculations are excellent over the fluid dynamics regime from laminar to supersonic flow.

Based on all of these analyses, the SIMMER hydrodynamics formulation is felt to be verified[84] for the expansion-type problems, but verification of the rate effects in expansion problems is incomplete. Recently, SIMMER has been

used to calculate several experiments having significant rate effects. These include Oak Ridge National Laboratory (ORNL) FAST/CRI experiments,[85] the SRI 1/30-scale flashing-source experiment,[80] Sandia prompt-burst excursion (PBE) experiments,[86] and the Purdue OMEGA flashing-source experiments.[87] In the last case, good agreement could be obtained only when a nucleation-site density model was added. In most other cases, the comparisons are sufficiently reasonable (given limited experimental data) that model changes are not justified.

Overall, SIMMER has been quite thoroughly tested for the bubble expansion problems. One remaining problem with the SIMMER modeling framework is that the Eulerian solution leads to "numerical" mixing. The mixing effect is dependent on mesh-cell size and is exaggerated when large mesh cells are used because the necessary averaging of quantities within the cells tends to equilibrate temperatures too rapidly (or at least nonmechanistically). This effect may not be significant in the small-scale experiment analyses because of the necessarily small mesh cells used, but it could be a factor in extrapolating "verified" rate effects models to full scale. Testing for other than expansion problems, such as those of the transition phase, has been very limited. One exception is that SIMMER was used to calculate,[88] relatively successfully, the TREAT R7 test for the full span of sodium boiling, cladding relocation, and fuel motion.

Verification of disassembly codes has been complicated by the fact that no disassembly transient experiments have been performed on LMFBRs. There have been, however, a limited number of disassembly tests performed on other reactor types. Although these reactors differed markedly from an LMFBR, the data obtained have provided a basis for experimental validation of LMFBR disassembly codes. The most applicable of these tests are the KIWI-TNT,[89] SNAPTRAN-2,[90] and SNAPTRAN-3[91] experiments.

The SNAPTRAN experiments were performed on SNAP 2/10A reactors. These reactors had small zirconium-hydride cores with fully enriched uranium. The SNAPTRAN-2 test was performed in the open atmosphere with no coolant present in the core. Rapid reactivity insertion was achieved by modifying the normal beryllium control-drum drive mechanisms to allow for extremely high-speed rotation. A total reactivity of $4.91 was inserted. In the SNAPTRAN-3 experiment, the beryllium reflector/control assembly was replaced by a neutron-absorbing metal sleeve. The core-sleeve assembly was then placed in a large tank of water. A prompt-critical excursion was initiated by the rapid removal of the sleeve, with the consequential increase in neutron reflection. A net reactivity of $3.60 was achieved upon sleeve removal. The core was full of cold coolant during this test.

The KIWI-TNT test was the most energetic disassembly experiment available. It was performed on a modified KIWI-B-4E reactor. The core was fueled with fully enriched uranium-dicarbide beads dispersed in graphite assemblies. The excursion was initiated by the rapid rotation of beryllium control drums that resulted in a total reactivity insertion of $8.30. The test was performed with no coolant present in the core.

All three of these tests were analyzed with the VENUS-II code.[92] To apply the code to these reactors, modifications were made to the equation of state and the heat-capacity functions to account for the core materials not normally found in LMFBRs. All other aspects of the code, including hydrodynamics and point kinetics calculations, were used without modification.

The VENUS-II code accurately predicted the power history and total fission energy release in these three experiments. The most important calculated

results, the total fission energy releases, are compared to the measured values in Table I. The calculated fission energies for the two SNAPTRAN tests fell within the uncertainty range of the experimental data, but the code overpredicted the KIWI-TNT experiment by 25%. Additional analysis of KIWI-TNT, however, showed this discrepancy could readily be explained by heat-transfer effects associated with the reactor's beaded fuel (a complication not present in an LMFBR).

Numerous parametric calculations also were performed that demonstrated the relative insensitivity of the VENUS-II results to reasonable uncertainties in the key parameters. In the SNAPTRAN experiments, the most sensitive parameters were those related to the temperature feedback effects that were dominant in these excursions. This is similar to the situation found in energetic LMFBR excursions where Doppler feedback is usually the dominant effect.

Barring unforeseen feedback effects, the code should be even more accurate when applied to energetic LMFBR transients.[93] This is because the key parameters (heat capacity, temperature coefficient, and equation of state) are relatively better known for an LMFBR. Thus, the good agreement observed in these experimental comparisons lends considerable confidence to VENUS-II LMFBR disassembly analyses.

The REXCO codes have received thorough testing of both hydrodynamics and structural methods by comparisons to PBTF scale model experiments performed at SRI[94] and to SNR-300 scale model experiments performed at Ispra.[95] Figure 13 shows REXCO- and ICECO-calculated plastic deformations for a thin vessel Ispra experiment. This indicates quite good agreement, and similarly good agreement was obtained in the other comparisons noted. REXCO- and ICECO-calculated hydrodynamics parameters (pressures, fluid impulses) both show good agreement, which is interesting because of the large difference in the numerical formulations, REXCO being an explicit Lagrangian code and ICECO being a semi-implicit Eulerian code.

Overall, experimental verification of HCDA analysis codes has proceeded slowly. Generally, hydrodynamics and structural dynamics models dealing with relatively clearly defined problems, such as sodium boiling and damage consequences (such as vessel deformation), have fared well in experimental comparisons. In more complex phenomenological situations, such as fuel pin disruption, combined fuel and cladding motion, and transition phase dynamics, treatment of complicated and changing geometries and multicomponent multiphase flows makes mechanistic modeling much more difficult. This, coupled with a lack of adequate data from in-reactor experiments and the near-impossibility of performing multicomponent simulant experiments with internal heat generation, means that

TABLE I

COMPARISON OF VENUS-II CALCULATIONS WITH EXPERIMENTAL DATA

Test	Experimental Energy Release (MW-s)	Calculated Energy Release (MW-s)
SNAPTRAN-2	38.0 - 47.3	47.0
SNAPTRAN-3	32.7 - 61.3	33.7
KIWI-TNT	8090.0 - 9889.0	12350.0

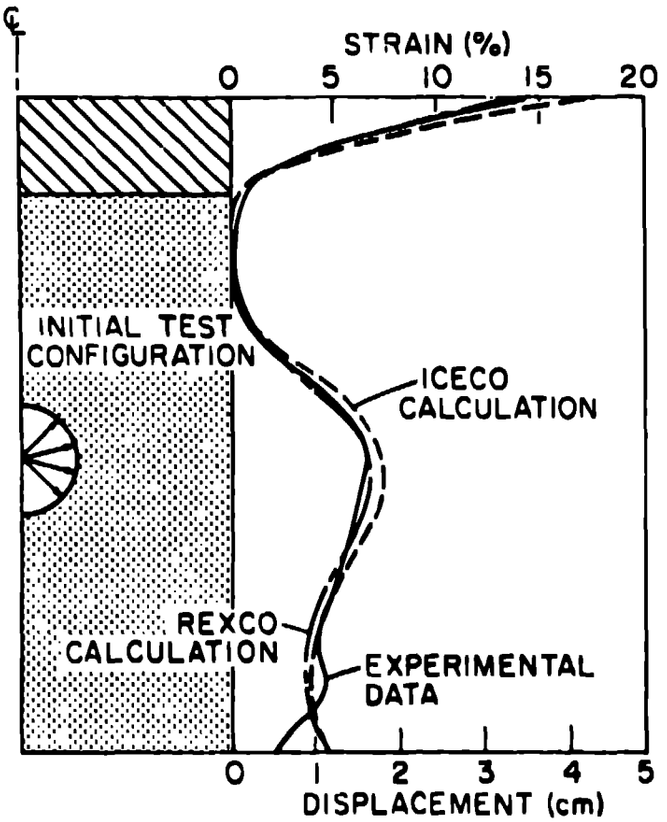

Fig. 13. REXCO/ICECO comparisons for deformations of a thin test vessel.

total verification is improbable for some time. However, most of the modeling is at least technically credible, and the codes still can be used to determine the sensitivity of important results to modeling uncertainties. Also, some conclusions on cladding or fuel motions based on specific analyses can be verified by integral reactivity measurements, such as in the SLSF loop, rather than by verifying the modeling itself. Of course, care must be taken in extrapolating such conclusions to the full-scale reactor case.

9. CONCLUSIONS

The combination of SAS3D or SAS4A, SIMMER-II, and REXCO or ICECO, as representing the state of the art in HCDA analysis techniques, generally can provide a reasonable treatment of complete HCDA sequences. Other codes, developed in the US or in other countries, also can fit in this combination of state-of-the-art codes; but SAS, SIMMER, and REXCO provide at least one set of detailed codes for straight-through calculations of most disruptive accident sequences. Much remains to be done in improving models and computational efficiencies and in verifying the codes, but defensible analyses are feasible.

ACKNOWLEDGEMENTS

Our acknowledgements and apologies go to the many co-authors on our previous papers from which much of this material was drawn. The descriptions of numerical methods, largely provided by D. P. Weber in Ref. 96, were particularly valuable. We also acknowledge the pioneering contributions made by key people in the development of the state-of-the-art mechanistic HCDA analysis techniques discussed here. Some of these are R. B. Nicholson, F. E. Dunn, T. J. Heames, W. R. Bohl, L. L. Smith, J. E. Boudreau, C. R. Bell, and Y. Chang. Most importantly, the efforts of G. J. Fischer in instilling the idea that mechanistic analysis is both worthwhile and possible and his early leadership in the development of analysis techniques, were an enormous contribution.

APPENDIX A

SOME BASIC CONCEPTS IN NUMERICAL ANALYSIS

A.1 INTRODUCTION

Several numerical concepts and methods are referred to in the reactor safety computer code descriptions in Chapters 13 and 19. This appendix provides introductory background material on some of the main concepts.

A.2 REVIEW OF BASIC CONCEPTS

Finite difference equations. Finite difference techniques are used to transform differential equations into coupled sets of algebraic equations that can be solved with the standard arithmetic and logical operations available in digital computers. In carrying this out, a network of mesh (or grid) points is established throughout the domain occupied by the independent variables. The variables and equation solution then are defined at the mesh points or at interpolated positions between them. The equations then are written for these mesh points with the differential operators approximated by difference expressions involving the variables at neighboring mesh points.

Eulerian vs Lagrangian coordinates. Fluid dynamics equations can be solved numerically in two different types of grid mesh coordinate systems.[97] In the Lagrangian approach, the grid mesh is assumed to move with the fluid. Thus, a given mesh cell contains the same fluid throughout the calculation. This approach is depicted in Fig. A.1 where we illustrate the deformation that might result from an applied central pressure. As long as the displacements are relatively small, this approach can work very well. As displacements become large, however, the mesh cells can become highly distorted. In fact, neighboring mesh points can even cross over one another, resulting in mesh cells with an "hourglass" shape. When these large distortions occur, the results typically are inaccurate. This difficulty can be circumvented somewhat

by techniques that periodically regularize the grid. These techniques are generally quite complicated and introduce errors into the calculation each time they are applied.

The use of Lagrangian coordinates can offer distinct advantages for certain types of small-displacement hydrodynamics calculations, however. For example, material interfaces can be readily retained. Also, the mathematical formulation is quite simple. This is illustrated in the development of the VENUS disassembly code finite difference equations presented in Appendix B of this chapter. The problem solved by VENUS is well suited to Lagrangian coordinates because core material displacements of only a few centimeters are typically required to terminate a prompt-critical neutronics excursion. The Lagrangian coordinate approach also was used in the early versions of the REXCO damage evaluation code. A later version of the code incorporated mesh cell renormalization to facilitate the analysis of larger displacements.

In the Eulerian approach, the grid mesh is fixed in space and the fluid is allowed to move from one mesh cell to another in response to pressure gradients. This is illustrated in Fig. A.2. This type of approach is much better suited to hydrodynamics problems where large material displacements are calculated. For example, it has been used exclusively in the LMR systems codes discussed in Chapter 13. All of the more recent LMFBR codes discussed in this chapter are also Eulerian.

The Eulerian approach does have some inherent problems. For example, interfaces are difficult to resolve precisely. There is also a tendency for artificial material diffusion. As material diffuses into a mesh cell, it is immediately homogenized throughout the cell (in basic Eulerian treatments). It

Fig. A-1. Illustration of Lagrangian coordinate approach.

Fig. A-2. Illustration of Eulerian coordinate approach.

can then start diffusing through the other mesh cell boundaries during the next time step. This can result in small amounts of material diffusing through the grid much more rapidly than the material can physically move.

Some more complicated schemes have been developed that try to combine the advantages of both approaches. In one such scheme, the Particle-in-Cell (PIC) method,[98] the continuous fluid is replaced by a set of discrete Lagrangian mass points called particles. The motion of these particles through a fixed Eulerian mesh is calculated.

Explicit vs implicit. To illustrate the difference between explicit and implicit differencing schemes, consider the following parabolic equation[99]

$$\frac{\partial^2 u(x,t)}{\partial x^2} = \frac{\partial u(x,t)}{\partial t} \quad \alpha = \text{constant.} \tag{A-1}$$

If we wish to solve for u(x,t) numerically, we can superimpose a grid mesh with grid line indices of j and k in the t and x directions, respectively. This notation is illustrated in Fig. A.3. Let the solution at point (j,k) be denoted as $u_{j,k}$.

Suppose we have the solution up to t_j and we now wish to advance it to t_{j+1}. To do this we must put Eq. (A-1) into finite difference form. One way to do this is to start at point (j,k) and use the following central difference expression for $\partial^2 u/\partial x^2$:

$$\frac{\partial^2 u}{\partial x^2} \approx \left[\frac{u_{j,k+1} - u_{j,k}}{\Delta x} - \frac{u_{j,k} - u_{j,k-1}}{\Delta x}\right] \cdot \frac{1}{\Delta x} = \frac{u_{j,k+1} - 2u_{j,k} + u_{j,k-1}}{(\Delta x)^2} .$$

If we use a simple forward difference for the time derivative, we obtain

$$\frac{\partial u}{\partial t} \approx \frac{u_{j+1,k} - u_{j,k}}{\Delta t} .$$

Equation (A-1) then becomes

$$u_{j,k+1} - 2u_{j,k} + u_{j,k-1} = \frac{(\Delta x)^2}{\alpha \Delta t}(u_{j+1,k} - u_{j,k}) . \tag{A-2}$$

This expression involves the points in the grid mesh depicted in Fig. A.3.

All the quantities with subscript j are known; therefore the only unknown is $u_{j+1,k}$ (which is point D in Fig. A.3). Thus, Eq. (A-2) can be explicitly solved for $u_{j+1,k}$. This type of differencing approach is therefore referred to as explicit.

The main difficulty with explicit techniques is one of stability. For example, it can be shown that solutions obtained with Eq. (A-2) will only remain stable if

Fig. A-3. Grid mesh representing explicit differencing approach.

Fig. A-4. Grid mesh representing implicit differencing approach.

$$\Delta t < \frac{(\Delta x)^2}{2\nu} .$$

Typically, this criterion forces the time-step size to be much smaller than would be required to control the truncation error. Thus, although explicit techniques are computationally simple, the restriction on time-step size only makes them practical for problems that cover short-time intervals. An explicit approach can be successfully used in reactor disassembly codes such as VENUS, because a typical disassembly calculation only covers a time interval of several milliseconds or less.

Now consider a new difference representation that is centered on point $(j+1,k)$. If $\partial^2 u/\partial x^2$ is approximated again with a central difference expression, but $\partial u/\partial t$ is now represented by a backward difference expression, the result is

$$\frac{u_{j+1,k+1} - 2u_{j+1,k} + u_{j+1,k-1}}{(\Delta x)^2} = \frac{1}{\nu} \frac{(u_{j+1,k} - u_{j,k})}{\Delta t} . \qquad \text{(A-3)}$$

The points involved in this difference scheme are shown in Fig. A.4. Now the values of u at points A, B, and C are all unknown. Although Eq. (A-3) cannot be solved explicitly for these unknowns, it can be written for all of the points k-1, 2, ..., n, resulting in n linear equations in the n unknowns $u_{j+1,k}$. These equations can then be solved with standard numerical matrix techniques. Such an approach is said to be implicit.

Although computationally more complex, implicit techniques can typically tolerate much larger time-step sizes than explicit techniques. In fact, most purely implicit formulations can be shown to be stable for any time-step size. In the semi-implicit approaches commonly used in reactor safety codes[100] (these usually use a donor-cell technique where some of the differencing depends on the direction of the flow), the time-step size must satisfy the so-called Courant condition,

$$\Delta t < \frac{\Delta x}{v} ,$$

where v is the material velocity. This is much less restrictive than is obtained for explicit approaches.

Stevenson page. 33
Fig. A-3 top left of page
Please reduce to 77% of original

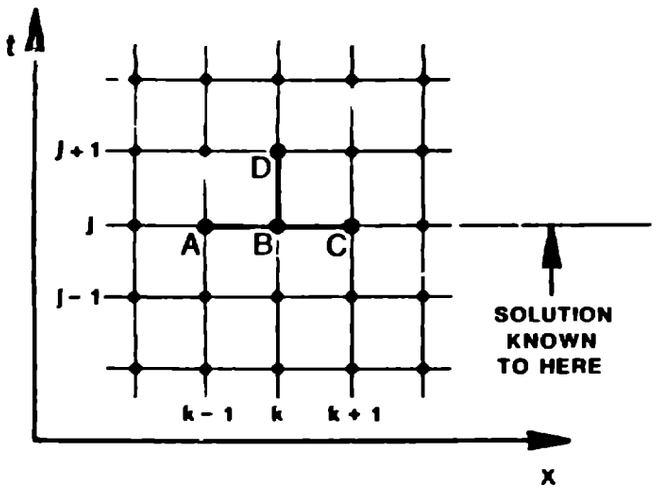

Stevenson page 33
Fig. A-4 top right of page
Please reduce to 77% of original

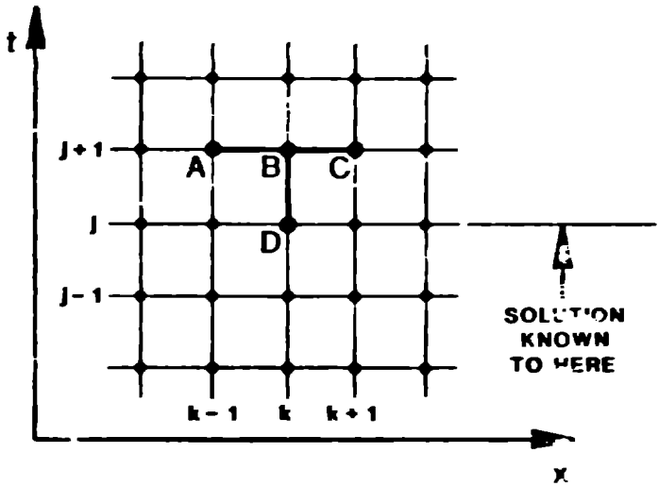

A number of advanced implicit techniques have been developed. One that has found considerable application in reactor safety codes is the Implicit Continuous-fluid Eulerian (ICE) technique.[51] This technique was developed for multidimensional flows at all flow speeds. It features an implicit treatment of density in the equation of state and of the density and velocity in the mass equation.

APPENDIX B

HYDRODYNAMICS DIFFERENCE EQUATIONS AND SOLUTION STRATEGY FOR VENUS AND REXCO CODES

B.1 INTRODUCTION

This appendix gives a detailed example of the different equations and solution strategy used in a reactor safety computer code. The appendix in Chapter 13 discusses an example of an implicit-Eulerian technique, so we have chosen to develop an explicit-Lagrangian example in this appendix. For this purpose, we will discuss the numerical techniques used to solve the hydrodynamics equations in the original VENUS (disassembly) and REXCO (damage evaluation) codes. This method was previously developed and used at LASL.[98] The development prescribed here will follow that given in Ref. 101.

B.2 DIFFERENTIAL EQUATIONS

As the hydrodynamics equations are solved in Lagrangian coordinates, mass conservation is expressed merely by

$$\rho = \frac{\rho_o V_o}{V_t} \quad , \tag{B-1}$$

where ρ and V_t are the density and total volume of a given mesh cell and ρ_o and V_o are the initial values. Equation (B-1) simply follows from the fact that each mesh cell contains the same material throughout the calculation.

The equations are solved in two-dimensional (r-z) geometry resulting in the following momentum equations:

$$\ddot{r} = -\frac{1}{\rho}\frac{\partial P}{\partial r} \qquad \text{and} \qquad \ddot{z} = \frac{1}{\rho}\frac{\partial P}{\partial z} \quad . \tag{B-2}$$

Here, r and z are the Eulerian coordinates of a given point in the Lagrangian grid mesh, P is the pressure, and the dots refer to time differentiation. Thus, these equations give the acceleration of the Lagrangian grid points that result from appropriately averaged pressure gradients.

B.2 DIFFERENCE EQUATIONS

In developing the difference equations, the notation depicted in Fig. B.1 will be used. Because the Lagrangian grid moves with the fluid, it will become distorted as illustrated in the figure. The mesh points (the intersections of Lagrangian grid lines) are identified by a pair of integers (I,J). The mesh cells are identified by the integers of the lower left mesh point (in the undeformed Lagrangian meshes); for example, the mesh zone ODHA is identified as zone (I,J). Positions, velocities, and accelerations are assumed to be associated with the mesh points; they are identified by the mesh-point integers as subscripts. Specific volumes, densities and pressures, strains, and internal energies are assumed to be associated with the cells; they are identified by the mesh cell numbers as subscripts. The times t, $t + \Delta t$, and $t + \Delta t/2$ are identified by superscripts n, $n + 1$, and $n + \frac{1}{2}$. The latter also is used to identify the change in a quantity between t^n and t^{n+1}. Where appearing, the superscript 0 denotes the initial value of a quantity at the start of the problem.

In the Lagrangian formulation, mass conservation is automatically satisfied. However, a mass equation is needed for the computation of the new density , which is used in the momentum equations and in the equation of state. This computation is performed as follows:

Fig. B-1. A typical mesh point (I,J) with the adjacent zones and points, illustrating the notation used in the finite-difference equations.

Fig. B-1 bottom of page

Please reduce to 77% or original

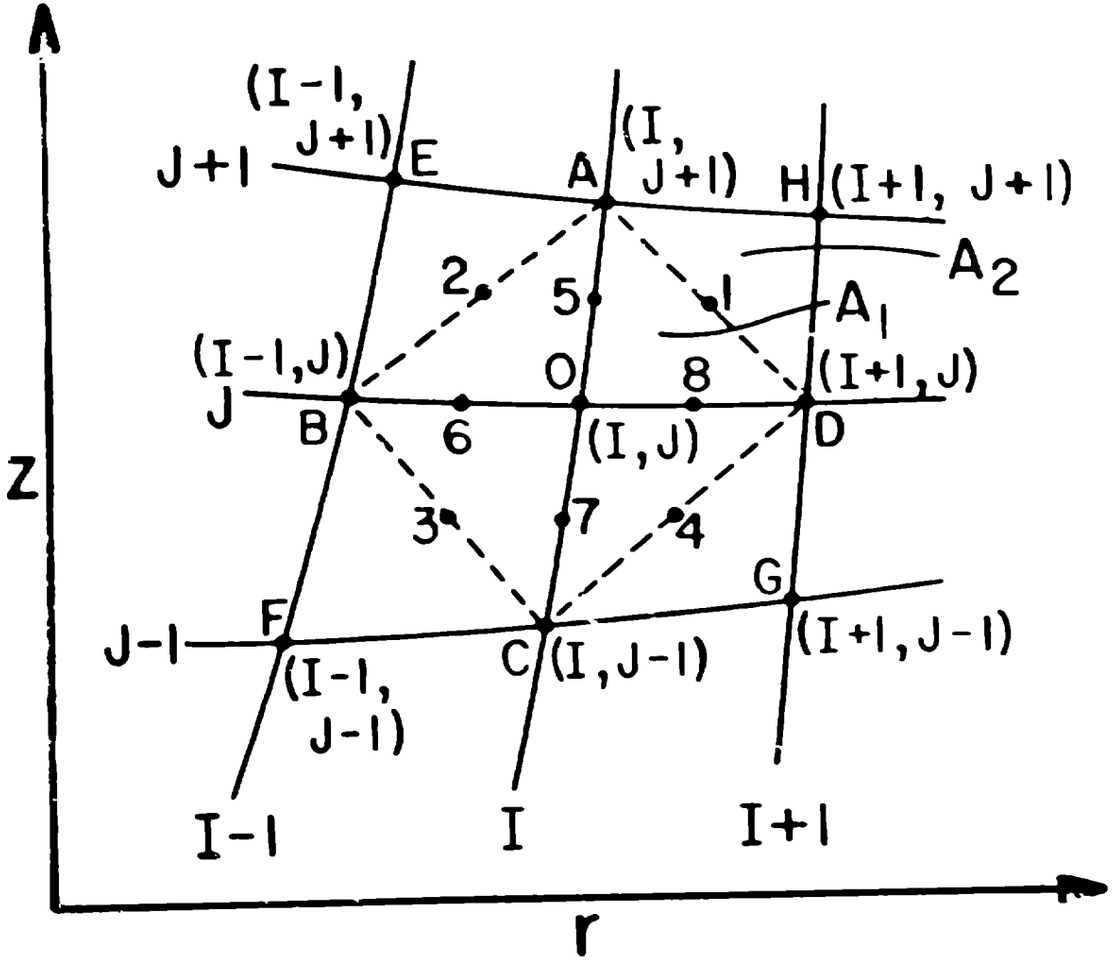

The area of the deformed mesh ODHA is the sum of two triangles AOD and AHD:

$$A_{I,J} = A_1 + A_2 ,$$

where

$$A_1 = \frac{1}{2}\,\overline{OD} \times \overline{OA} = \frac{1}{2}[(r_{I+1,J} - r_{I,J})(z_{I,J+1} - z_{I,J}) - (r_{I,J+1} - r_{I,J})(z_{I+1,J} - z_{I,J})] , \tag{B-3}$$

and

$$A_2 = \frac{1}{2}\,\overline{HA} \times \overline{HD} = \frac{1}{2}[(r_{I,J+1} - r_{I+1,J+1})(z_{I+1,J} - z_{I+1,J+1}) - (r_{I+1,J} - r_{I+1,J+1})(z_{I,J+1} - z_{I+1,J+1})] . \tag{B-4}$$

Substitution of Eqs. (B-1) and (B-2) for A_1 and A_2 gives

$$A_{I,J} = \frac{1}{2}[(z_{I+1,J+1} - z_{I,J})(r_{I+1,J} - r_{I,J+1}) - (r_{I+1,J+1} - r_{I,J})(z_{I+1,J} - z_{I,J+1})] . \tag{B-5}$$

The volume V of a quadrilateral is calculated from

$$V_{I,J} = A_{I,J} \cdot \bar{r}_{I,J} , \tag{B-6}$$

where $\bar{r}_{I,J}$ is the radius of the centroid of the area $A_{I,J}$. A reasonable approximation for moderate distortions is

$$\bar{r}_{I,J} = \frac{1}{4}(r_{I,J} + r_{I,J+1} + r_{I+1,J} + r_{I+1,J+1}) . \tag{B-7}$$

Next, the finite-difference form of Eq. (B-1) is just

$$\left(\frac{\partial P}{\partial z}\right)_{I,J} = \frac{P^n_{I+1,J} - P^n_{I,J}}{z^n_{I+1,J} - z^n_{I,J}} . \tag{B-8}$$

The momentum equations are put into finite-difference using the Wilkins Method. This is a Taylor's expansion between points 0 and 5, 0 and 6, 0 and 7, and 0 and 8, which yields four equations of the form

$$P_5 = P_0 + (z_5 - z_0)\frac{\partial P}{\partial z} + (r_5 - r_0)\frac{\partial P}{\partial r} + \frac{1}{2}(z_5 - z_0)^2 \frac{\partial^2 P}{\partial z^2} + (z_5 - z_0)(r_5 - r_0)\frac{\partial^2 P}{\partial z \partial r} + \frac{1}{2}(r_5 - r_0)^2 \frac{\partial^2 P}{\partial r^2} + \ldots ,$$

where terms of third and higher order in $(z_5 - z_0)$ and $(r_5 - r_0)$ have been omitted. The system is overdetermined for $\partial P/\partial z$ and $\partial P/\partial r$. One method of removing the overdeterminacy is to solve first for $(P_5 - P_7)$ and $(P_6 - P_8)$, which gives

$$P_5 - P_7 = (z_5 - z_7)\frac{\partial P}{\partial z} + (r_5 - r_7)\frac{\partial P}{\partial r} + \frac{\partial^2 P}{\partial z^2}(z_5 - z_7)_{z57}$$

$$+ \frac{\partial^2 P}{\partial r^2}(r_5 - r_7)_{r57} + \frac{\partial^2 P}{\partial z\,\partial r}\left[(z_5 - z_7)_{r57}\right.$$

$$\left. + (r_5 - r_7)_{z57}\right] + \cdots$$

and

$$P_6 - P_8 = (z_6 - z_8)\frac{\partial P}{\partial z} + (r_6 - r_8)\frac{\partial P}{\partial r} + \frac{\partial^2 P}{\partial z^2}(z_6 - z_8)_{z68}$$

$$+ \frac{\partial^2 P}{\partial r^2}(r_6 - r_8)_{r68} + \frac{\partial^2 P}{\partial z\,\partial r}\left[(z_6 - z_8)_{r68}\right.$$

$$\left. + (r_6 - r_8)_{z68}\right] + \cdots,$$

where

$$(z)_{z57} = \frac{1}{2}(z_5 + z_7) - z_0, \text{ etc.},$$

are measures of the asymmetry of the mesh. Second- and higher-order terms in the mesh size -- i.e., $(z_5 - z_7)$, $(r_5 - r_7)$, etc. -- are retained.

The above equations are then solved for the results

$$\left.\begin{aligned}\frac{\partial P}{\partial z} &= \frac{1}{A_3}\left[(P_5 - P_7)(r_6 - r_8) - (P_6 - P_8)(r_5 - r_7)\right] + P_z \\ \text{and} \\ \frac{\partial P}{\partial r} &= \frac{1}{A_3}\left[(P_5 - P_7)(z_6 - z_8) - (P_6 - P_8)(z_5 - z_7)\right] + P_r\end{aligned}\right\}, \quad (B\text{-}4)$$

where

$$A_3 = \frac{1}{2}\left[(z_5 - z_7)(r_6 - r_8) - (z_6 - z_8)(r_5 - r_7)\right]$$

represents the area of the quadrilateral 5-6-7-8. The remaining terms, P_z and P_r, involve products of the mesh size and the $(\cdots)$'s. If the mesh is nearly symmetric, these terms are negligible compared to those that have been retained.

We substitute Eq. (B-4) into the momentum equations, neglect the remaining terms, and write

$$P_5 = \frac{1}{2}(P_{I,J} + P_{I-1,J}), \quad P_6 = \frac{1}{2}(P_{I-1,J} + P_{I-1,J-1}),$$

$$p_7 = \frac{1}{2}(p_{I-1,J-1} + p_{I,J-1}), \quad p_8 = \frac{1}{2}(p_{I,J} + p_{I,J-1}),$$

$$r_5 = \frac{1}{2}(r_{I,J+1} + r_{I,J}), \quad r_6 = \frac{1}{2}(r_{I,J} + r_{I-1,J}),$$

$$r_7 = \frac{1}{2}(r_{I,J} + r_{I,J-1}), \quad r_8 = \frac{1}{2}(r_{I+1,J} + r_{I,J}),$$

$$z_5 = \frac{1}{2}(z_{I,J+1} + z_{I,J}), \quad z_6 = \frac{1}{2}(z_{I,J} + z_{I-1,J}),$$

$$z_7 = \frac{1}{2}(z_{I,J} + z_{I,J-1}), \text{ and } z_8 = \frac{1}{2}(z_{I,J} + z_{I+1,J}),$$

we obtain

$$\ddot{r}_{I,J} = \frac{-1}{(\rho A)_{I,J}}[(p_{I,J} - p_{I-1,J-1})(z_{I,J+1} - z_{I,J-1} + z_{I-1,J} - z_{I+1,J}) - (p_{I-1,J} - p_{I,J-1})(z_{I,J+1} - z_{I,J-1} + z_{I+1,J} - z_{I-1,J})]$$

and

$$\ddot{z}_{I,J} = \frac{1}{(\rho A)_{I,J}}[(p_{I,J} - p_{I-1,J-1})(r_{I,J+1} - r_{I,J-1} + r_{I-1,J} - r_{I+1,J}) - (p_{I-1,J} - p_{I,J-1})(r_{I,J+1} - r_{I,J-1} + r_{I+1,J} - r_{I-1,J})] \quad . \quad \text{(B-10)}$$

where

$$(\rho A)_{I,J} = A_{I,J}\rho_{I,J} + A_{I-1,J}\rho_{I-1,J} + A_{I-1,J-1}\rho_{I-1,J-1} + A_{I,J-1}\rho_{I,J-1} .$$

Since time index is specified in Eq. (B-10), the implication being that all variables are prescribed for the same time.

B.4 SOLUTION PROCEDURE

It is assumed that all calculations are performed up through cycle $(n-1)$, so that for all points and zones there are available the values of r^n, z^n, $\dot{r}^{n-\frac{1}{2}}$, $\dot{z}^{n-\frac{1}{2}}$, A^n, V^n, and p^n.

Next, the accelerations at time n are explicitly calculated from Eq. (B-10). These accelerations are then used to advance the velocities of all points to time $n+\frac{1}{2}$.

$$\left.\begin{aligned} \dot{r}^{n+\frac{1}{2}} &= \dot{r}^{n-\frac{1}{2}} + \ddot{r}^{n}\left[\tfrac{1}{2}(\Delta t^{n+\frac{1}{2}} + \Delta t^{n-\frac{1}{2}})\right] \\ \text{and} \\ \dot{z}^{n+\frac{1}{2}} &= \dot{z}^{n-\frac{1}{2}} + \ddot{z}^{n}\left[\tfrac{1}{2}(\Delta t^{n+\frac{1}{2}} + \Delta t^{n-\frac{1}{2}})\right] \end{aligned}\right\} , \qquad (3\text{-}11)$$

where

$$\Delta t^{n+\frac{1}{2}} = t^{n+1} - t^{n}$$

and

$$t^{n-\frac{1}{2}} = t^{n} - t^{n-1} .$$

These velocities, in turn, are used to advance the coordinates of all points to time n + 1.

$$\left.\begin{aligned} r^{n+1} &= r^{n} + \dot{r}^{n+\frac{1}{2}}\Delta t^{n+\frac{1}{2}} \\ \text{and} \\ z^{n+1} &= z^{n} + \dot{z}^{n+\frac{1}{2}}\Delta t^{n+\frac{1}{2}} \end{aligned}\right\} . \qquad (3\text{-}12)$$

Once the coordinate positions have been advanced, the mesh-cell volumes are recalculated. The mesh-cell densities are updated using Eq. (3-8), and are used, in turn, to calculate the new mesh-cell pressures. This completes one time step in the hydrodynamics calculation.

REFERENCES

1. H. A. Bethe and J. H. Tait, "An Estimate of the Order of Magnitude of the Explosion When the Core of a Fast Reactor Collapses," UKAEA-RHM(56)/113 (1956).

2. D. R. MacFarlane, Ed., "SASLA, A Computer Code for the Analysis of Fast Reactor Power and Flow Transients," Argonne National Laboratory report ANL-7607 (1970).

3. F. E. Dunn, G. J. Fischer, T. J. Heames, P. Pizzica, N. A. McNeal, W. R. Bohl, and S. M. Prastein, "The SAS2A LMFBR Accident Analysis Computer Code," Argonne National Laboratory report ANL-8138 (1975).

4. M. G. Stevenson, W. R. Bohl, F. E. Dunn, T. J. Heames, G. Hoppner, and L. L. Smith, "Current Status and Experimental Basis of the SAS LMFBR Accident Analysis Code System," Proc. ANS Conf. Fast Reactor Safety, Beverly Hills, California, 1974, USAEC-CONF 740401, p. 1303.

5. J. E. Cahalan, et al., "The Status and Experimental Basis of the SAS4A Accident Analysis Code System," Proc. Int. Mtg. on Fast Reactor Safety Technology, Seattle, 1979 (American Nuclear Society, LaGrange, Illinois, 1979), Vol. II, pp 603-614.

6. W. T. Sha and T. H. Forbes, "VENUS: A Two-Dimensional Coupled Neutronics-Hydrodynamics Computer Program for Fast-Reactor Power Excursions," Argonne National Laboratory report ANL-7701 (October 1970).

7. J. F. Jackson and P. B. Nicholson, "VENUS-II: An LMFBR Disassembly Program," Argonne National Laboratory report ANL-7951 (1972).

8. C. R. Bell, et al., "SIMMER-I: An Sn, Implicit, Multifield, Multicomponent, Eulerian Recriticality Code for LMFBR Disrupted Core Analysis," Los Alamos Scientific Laboratory report LA-UR-76-6667-MS (January 1977).

9. L. L. Smith, "SIMMER-II: A Computer Program for LMFBR Disrupted Core Analysis," Los Alamos Scientific Laboratory report LA-7515-M (October 1978).

10. Y. M. Chang and J. Gvildys, "REXCO-HEP: A Two-Dimensional Code for Calculating the Primary System Response in Fast Reactors," Argonne National Laboratory report ANL-75-19 (June 1975).

11. A. E. Waltar, et al., "MELT-III, A Two-Dimensional, Thermal-Hydraulics Computer Program for Fast Reactor Safety Analysis," Hanford Engineering Development Laboratory report HEDL-TME 77-57 (December 1976).

12. J. J. Sienicki and P. B. Abramson, "The TWOPHL Strategy and the Coupled Compressible/Incompressible Flow Problem," Proc. of the Topical Meeting on Computational Methods in Nuclear Engineering, Williamsburg, Virginia, April 1979, pp. 1-69.

13. D. P. Weber, et al., "VENUS-III: An Eulerian Disassembly Code," Trans. Am. Nucl. Soc. 21, 219 (1975).

14. A. E. Waltar and A. Padilla, Jr., "Mathematical and Computational Techniques Employed in the Deterministic Approach to Liquid-Metal Fast Breeder Reactor Safety," Proc. Nat. Topical Mtg. of the ANS Mathematics and Computation Division, Tucson, 1977 (Am. Nuc. Society, LaGrange Park, Illinois 1977) Vol. 64, No. 2, pp. 418-451.

15. D. D. Freeman, "Coupling of Dynamics Calculations i[n] FREADM Code," Proc. Conf. Effective Use of Computers in the Nucl. Industry, Knoxville, Tennessee, April 1969, USAEC Report CONF 690401.

16. M. G. Stevenson and B. E. Bingham, "TART: An LMFBR Transient Anal[ysis] Project," in Proc. Conf. Effective Use of Computers in the Nucl. [In]dustry, Knoxville, Tennessee, April 21-23, 1969, USAEC Report CONF 690401, pp. 16-29.

17. N. Hirakawa, "MARS, A Two-Dimensional Excursion Code," Atomic Power Development Associates report APDA-198 (June 1967).

18. M. G. Stevenson and J. H. Scott, "The Effect of Noncoherence in Fast Reactor Sodium Voiding Accidents," Trans. American Nuclear Society, San Francisco, California, December 1-4, 1969 (American Nuclear Society, Hinsdale, Illinois, 1970) Vol. 2 pp. 905-906.

19. J. W. Stephenson, Jr. and R. B. Nicholson, "Weak Explosion Program," ASTRA 417-G.0 (1961).

20. D. Okrent, et al., "AX-1, A Computing Program for Coupled Neutronics-Hydrodynamics Calculations on the IBM-704," Argonne National Laboratory report ANL-5977 (1959).

21. R. B. Nicholson, "Methods for Determining the Energy Release in Hypothetical Fast Reactor Meltdown Accidents," Nuc. Sci. Engr. 18, 207 (1964).

22. W. J. McCarthy and D. Okrent, "Fast Reactor Kinetics," The Technology of Nuclear Reactor Safety, Vol. 1, Chapter 10 (1964).

23. E. P. Hicks and D. C. Menzies, "Theoretical Studies on the Fast Reactor Maximum Accident," Proc. Conf. Safety Fuels and Core Design in Large Fast Power Reactors, October 11-14, 1965; also Argonne National Laboratory report ANL-7120 (1965).

24. D. H. Cho, W. L. Chen, and R. W. Wright, "Pressure Pulses and Mechanical Work from Molten Fuel-coolant Interactions: A Parametric Study," Trans. Am. Nucl. Soc. 14, 290 (1971).

25. A. Padilla, Jr., "Analysis of Mechanical Work Energy for LMFBR Maximum Accidents," Nuclear Technology 12, 348 (1971).

26. J. Marchaterre, et al., "Work-Energy Characterization for Core-Disruptive Accidents," Proc. Conf. on Fast Reactor Safety and Related Physics, Chicago, Illinois, October 1976. CONF-761001, Vol. III, p. 1121.

27. P. L. Browne and M. S. Hoyt, "HASTI. -- A Numerical Calculation of Two-dimensional Lagrangian Hydrodynamics Utilizing the Concept of Space-dependent Time Steps," Los Alamos Scientific Laboratory report LA-3134 (1965).

28. L. Baker, Jr., "Core Debris Behavior and Interactions with Concrete," Nuclear Engineering and Design 42, No. 1, 137 (1977).

29. W. R. Bohl, J. E. Cahalan, and D. R. Ferguson, "An Analysis of the Unprotected Loss-of-Flow Accident in the Clinch River Breeder Reactors with an End-of-Equilibrium-Cycle Core," Argonne National Laboratory report ANL/RAS 77-15 (May 1977).

30. H. H. Hummel, Kalimullah, and P. A. Pizzica, "Physics and Pump Coast-down Calculations for a Model of a 4000 MWe Oxide-Fueled LMFBR," Argonne National Laboratory report ANL-76-77 (June 1976).

31. W. R. Bohl, "Some Recriticality Studies with SIMMER-II," Proc. Int. Mtg. on Fast Reactor Safety Technology, Seattle, 1979 (American Nuclear Society, LaGrange, Illinois, 1979) Vol. III, pp. 1415-1424.

32. C. R. Bell, J. E. Boudreau, J. H. Scott, and L. L. Smith, "Advances in the Mechanistic Assessment of Postdisassembly Energetics, Proc. Int. Mtg. on Fast Reactor Safety Technology, Seattle, 1979 (American Nuclear Society, LaGrange Park, Illinois, 1979) Vol. I, pp. 207-218.

33. A. E. Waltar, et al., "An Analysis of the Unprotected Transient Overpower Accident in the FTR," Hanford Engineering Development Laboratory report HEDL-TME 75-50 (June 1975).

34. W. R. Bohl and T. J. Hermes, "CLAZAS: The SAS3A Clad Motion Model," Argonne National Laboratory report ANL/RAS 74-15 (August 1974).

35. W. R. Bohl, "SLUMPY: The SAS3A Fuel Motion Model for Loss-of-Flow," Argonne National Laboratory report ANL/RAS 74-19 (August 1974).

36. D. R. MacFarlane, H. A. McNeal, D. Moseley, and C. K. Sanathanan, "Theoretical Studies of Fast Reactors During Sodium Boiling Accidents," Proc. of Int. Conf. on Safety of Fast Reactors, Aix-en-Provence, France (1967).

37. C. K. Youngdahl, "Fuel Element Deformation Model for Fast Reactor Accident Safety Study Code," Nucl. Eng. Design 15, 149-186 (1971).

38. A. Waterbo, "The DEFORM-II Mathematical Analysis of Plastic, Viscous, and Plastic Deformation of a Reactor Fuel Pin," Argonne National Laboratory report ANL-8041 (1973).

39. Bohl, op. cit., p. 2.

40. L. L. Smith, J. R. Travis, M. G. Stevenson, F. E. Dunn, and G. J. Fischer, "SAS/FCI, A Fuel-Coolant Interaction Model for LMFBR Meltdown Accident Analysis," Proc. ANS Topical Conf. on Mathematical Models and Computational Techniques for Analysis of Nuclear Systems, Ann Arbor, Michigan, 1973 (Am. Nuc. Society, LaGrange Park, Illinois, 1973) Vol. I.

41. W. R. Bohl and M. G. Stevenson, "A Fuel Motion Model for LMFBR Unprotected Loss-of-Flow Accident Analysis," Proc. ANS Topical Conf. on Mathematical Models and Computational Techniques for Analysis of Nuclear Systems, Ann Arbor, 1973 (American Nuclear Society, LaGrange Park, Illinois, 1973) Vol. II.

42. W. R. Bohl, "CLAP: A Cladding Action Program for LMFBR HCDA DF Analysis," Transactions ANS, Toronto, 1976 (American Nuclear Society, Hinsdale, Illinois, 1976) Vol. 23, pp. 368-369.

43. H. U. Wider, A. M. Tentner, and P. A. Pizzica, "The PLUTO2 Overpower Excursion Code and a Comparison with EPIC," Proc. of the Inter. Mtg. Fast Reactor Safety, Seattle, August 1979 (Am. Nuc. Society, LaGrange Park, Illinois) Vol. I, pp. 121-130.

44. A. M. Tentner and H. U. Wider, "LEVITATE - A Mechanistic Model for the Analysis of Fuel and Cladding Dynamics Under LOF Conditions for SAS4A," Proc. Int. Mtg. Fast Reactor Safety Technology, Seattle, 1979 (American Nuclear Society, LaGrange Park, Illinois, 1979) Vol. IV, pp. 1998-2007.

45. A. W. Cronenberg, H. K. Fauske, D. G. Bankoff, and D. F. Eggen, "A Single Bubble Model for Sodium Expulsion from a Heated Channel," Nucl. Engr. and Design 16, 285 (1971).

46. E. G. Schlechtendahl, "Theoretical Investigations on Sodium Boiling in Fast Reactors," Nucl. Sci. Engr. 41, 99 (1970).

47. G. Hopner and W. R. Bohl, "Analysis of Cladding and Fuel Motion in the R4 Experiment," Trans. Am. Nucl. Soc. 19, 239 (1974).

48. I. T. Hsang, et al., "Sodium Voiding Dynamics and Cladding Motion in a 37-Pin Fuel Assembly During an LOF Transient," Trans. Am. Nucl. Soc. 28, 445.

49. T. E. Fraft, et al., "Simulations of an Unprotected Loss-of-Flow Accident with a 37-Pin Bundle in the Sodium Loop Safety Facility," Proc. Int. Mtg. Fast Reactor Safety Technology, Seattle, 1979 (American Nuclear Society, LaGrange Park, Illinois) Vol. IV, pp. 1998-2007.

50. C. H. Lowers, L. L. Brinys, J. M. Kyser, and D. P. Weber, "An Improved Two-Component Sodium Voiding Model for the SAS4A Analysis Code," Proc. Int. Mtg. Fast Reactor Safety Technology, Seattle, 1979 (American Nuclear Society, LaGrange, Illinois, 1979) Vol. I, pp. 99-109.

51. F. H. Harlow and A. A. Amsden, "A Numerical Fluid Dynamics Calculation Method for all Flow Speeds," J. of Comp. Physics 8, 197 (1971).

52. W. R. Bohl, et al., "A Preliminary Study of the FFTF Hypothetical Flow Coastdown Accident," Argonne National Laboratory report ANL/RAS 71-39 (April 1972).

53. H. K. Fauske, Argonne National Laboratory, personal communication, July 1971.

54. Cahalan, op. cit., p. 609.

55. D. V. Gopinath and C. E. Dickerman, "Calculations of Coherence of Failure for Hypothetical Meltdown Accidents in an EBR-II-like Reactor," Argonne National Laboratory report ANL-6864 (1964).

56. L. W. Deitrich, "An Assessment of Early Fuel Dispersal in the Hypothetical Loss-of-Flow Accident," Proc. Int. Mtg. Fast Reactor Safety Technology, Seattle, 1979 (American Nuclear Society, LaGrange, Illinois, 1979) Vol. II, pp. 615-623.

57. R. D. Richtmeyer and K. W. Morton, Difference Methods for Initial-Value Problems (John Wiley and Sons, Inc., 1967).

58. Cahalan, op. cit., p. 609.

59. J. H. Scott and P. K. Mast, "Fuel Pin Failure Models and Fuel-Failure Thresholds for Core Disruptive Accident Analysis," Proc. Int. Mtg. on Fast Reactor Safety and Related Physics, Chicago, 1976, CONF-761001, Vol. III, pp. 1015-1026.

60. D. E. Simpson, A. E. Waltar, and A. Padilla, Jr., "Assessment of Magnitude and Uncertainties of Hypothetical Accidents for the FFTF," Hanford Engineering Development Laboratory report HEDL-TME 71-31 (1971).

61. P. G. Lorenzini and G. F. Flanagan, "An Evaluation of Fuel-Coolant Interaction During Disassembly of an LMFBR," Proc. Conf. New Developments in Reactor Mathematics and Applications, CONF-710302, Idaho Falls, Idaho (1971) p. 50.

62. A. W. Cronenberg, "A Thermodynamic Model for Molten UO_2-Na Interaction, Pertaining to Fast-Reactor Fuel-Failure Accidents," Argonne National Laboratory report ANL-7967 (1972).

63. F. E. Dunn, J. R. Travis, and L. L. Smith, "The PRIMAR-2 Primary Loop Module for the SASSA Code," Argonne National Laboratory report ANL-RAS 76-5 (March 1976).

64. Cahalan, op. cit., p. 606.

65. H. U. Wider, et al., "An Improved Analysis of Fuel Motion During an Overpower Excursion," Fast Reactor Safety, Beverly Hills, 1974, CONF-740401-P1, p. 1541.

66. P. A. Pizzica and P. Abramson, "FIC, A Computer Program for Fuel-Coolant Interactions," Int. Mtg. Fast Reactor Safety and Related Physics, Chicago, 1975, CONF-761001, Vol. III, pp. 979-987.

67. Wider, op. cit., p. 121.

68. J. VonNeumann and R. D. Richtmyer, "A Method for the Numerical Calculation of Hydrodynamic Shocks," J. Appl. Phys. 21, 3, 232 (1950).

69. F. O. Ott and D. A. Meneley, "Accuracy of the Quasistatic Treatment of Spatial Reactor Kinetics," Nucl. Sci. Eng. 36, 402 (1969).

70. D. A. Meneley et al., "A Fine Mesh Model for Fast-Reactor Analysis in Two Dimensions," Dynamics of Nuclear Systems, (University of Arizona Press, Tucson, Arizona, 1972) pp. 483-500.

71. W. T. Sha and A. E. Waltar, "An Integrated Model for Analyzing Disruptive Accidents in Fast Reactors," Nucl. Sci. and Engr. 44, 135-156 (1971).

72. M. G. Stevenson, "Nuclear Reactor Safety Quarterly Progress Report, October 1-December 30, 1979," Los Alamos Scientific Laboratory report LA-8099-PR (to be published).

73. A. A. Amsden and F. H. Harlow, "KACHINA: An Eulerian Computer Program for Multifield Fluid Flows," Los Alamos Scientific Laboratory report LA-5680 (1974).

74. J. E. Boudreau and J. F. Jackson, "Recriticality Considerations in LMFBR Accidents," Proc. Fast Reactor Safety Mtg, Beverly Hills, April 2-4, 1974, CONF-740401-P3.

75. Y. Chang, J. Wildys, and S. H. Fistedis, "Two-Dimensional Hydrodynamics Analysis for Primary Containment," Argonne National Laboratory report ANL-7498 (1969).

76. Chung-Yi Wang, "ICECO - An Implicit Eulerian Method for Calculating Fluid Transients in Fast-Reactor Containment," Argonne National Laboratory report ANL-75-81 (December 1975).

77. H. Y. Chu, et al., "A Generalized Eulerian Method in Reactor Containment Analysis and Its Comparison with Other Numerical Methods," Int. Mtg. on Fast Reactor Safety and Related Physics, Chicago, 1976, Vol. III, p 1285.

78. C. R. Bell and J. E. Boudreau, "SIMMER-I Accident Consequence Calculations," Trans. ANS, 1977, TRANSAO 27-1-1028, Vol. 27, pp. 555-556.

79. R. J. Tobin and D. J. Cagliostro, "Effects of Vessel Structures on Simulated HCDA Bubble Expansions," Stanford Research Institute technical report 5 (November 1978).

80. A. J. Suo-Anttila, "Analysis of Postdisassembly Expansion Experiments," Proc. Int. Mtg. on Fast Reactor Safety Technology, Seattle, 1979 (Am. Nuc. Society, LaGrange Park, Illinois, 1979) Vol. IV, pp. 1848-1857.

81. M. G. Stevenson, "Nuclear Reactor Safety Quarterly Progress Report, October 1-December 30, 1979," Los Alamos Scientific Laboratory report LA-8299-PR (to be published).

82. P. E. Rexroth, Los Alamos Scientific Laboratory, private communication, 1978.

83. J. E. Boudreau, et al., "A Critical Assessment of SIMMER-II Models," Los Alamos Scientific Laboratory report (to be published)

84. J. H. Scott, "Overview and Status of the SIMMER Testing Program," Proc. Int. Mtg. on Fast Reactor Safety Technology, Seattle, 1979 (Am. Nuc. Society, LaGrange, Illinois, 1979) Vol. I, pp. 197-206.

85. A. J. Suo-Anttila, Los Alamos Scientific Laboratory, private communication, 1979.

86. J. L. Tomkins, J. T. Hitchcock, and M. F. Young, "Prompt Burst Energetics (PBE) Experiment Analyses Using the SIMMER-II Computer Code," Proc. Int. Mtg. Fast Reactor Safety Technology, Seattle, 1979 (Am. Nucl. Society, LaGrange, Illinois, 1979) Vol. II, pp. 1001-1010.

87. A. J. Suo-Antilla, Los Alamos Scientific Laboratory, private communication, 1980.

88. W. R. Bohl, "A SIMMER-II Analysis of the R-7 Treat Test," Los Alamos Scientific Laboratory report NRRI/CR-0760, LA-7761-MS (April 1979).

89. L. D. P. King, et al., "Description of the KIWI-TNT Excursion and Related Experiments," Los Alamos Scientific Laboratory report LA-3350-MS (1966).

90. J. F. Jackson, W. F. Rhoades, and L. I. Moss, "Analysis of SNAPTRAN-1 and -2 Reactor Kinetics Experiments," Atomics International report NAA-SR-11850 (1967).

91. W. E. Kessler, et al., "SNAPTRAN 2/10A-3 Destructive Test Results," Phillips Petroleum Co., Atomic Energy Division report IDO-17019 (January 1965).

92. T. F. Pratt and J. F. Jackson, "Experimental Comparison Studies with the VENUS-II Disassembly Code," Proc. Conf. on Fast Reactor Safety and Related Physics, Chicago, 1976, CONF-761001, Vol. 3, p. 1134.

93. D. H. Barker, et al., "Improvement and Verification of Fast Reactor Safety Analysis Techniques: Progress Report," Department of Chemical Engineering, Brigham Young University report COO-2571-8 (1977).

94. S. H. Fistedis, et al., "Fast Reactor Containment Analysis, Recent Improvements, Applications, and Future Developments," Proc. Fast Reactor Safety Mtg., Beverly Hills, 1974, CONF-740401-P2, p. 763.

95. A. H. Marchertas, C. Y. Wang, and S. H. Fistedis, "A Comparison of ANL Containment Codes with SIR-300 Simulation Experiments," Int. Mtg. on Fast Reactor Methods, 1976, CONF-761001, Vol. III, p. 1324.

96. J. F. Jackson and D. P. Weber, "Hydrodynamics Methods in Fast Reactor Safety," Proc. Conf. on Computational Methods in Nuclear Engineering, Charleston, 1975, CONF-750413, Vol. I, pp. 27-52.

97. F. H. Harlow and A. A. Amsden, "Fluid Dynamics," Los Alamos Scientific Laboratory report LA-4700 (1971).

98. F. H. Harlow, "The Particle-In-Cell Method for Numerical Solution of Problems in Fluid Dynamics," Proc. Symposia in Applied Mathematics 15, 269 (1963).

99. R. W. Hornbeck, Numerical Methods (Quantum Publisher, Inc., New York, 1975).

100. Safety Code Development Group, "TRAC-PIA: An Advanced, Best-Estimate Computer Program for PWR LOCA Analysis," Los Alamos Scientific Laboratory report LA-7777-MS (May 1979).

101. P. L. Browne and M. S. Hoyt, "HASTL -- A Numerical Calculation of Two-dimensional Lagrangian Hydrodynamics Utilizing the Concept of Space-dependent Time Steps," Los Alamos Scientific Laboratory report LA-3324 (1965).